Y 3.N21/5:6/3340

GOVT. DOC.

NACA TN 3340

NATIONAL ADVISORY COMMITTEE FOR AERONAUTICS

BUSINESS AND TECHNICAL DEPT.

Mar 3'55

TECHNICAL NOTE 3340

GENERALIZATION OF GAS-FLOW-INTERFEROMETRY THEORY AND INTERFEROGRAM EVALUATION EQUATIONS FOR ONE-DIMENSIONAL DENSITY FIELDS

By Walton L. Howes and Donald R. Buchele

Lewis Flight Propulsion Laboratory
Cleveland, Ohio

Washington

February 1955

TABLE OF CONTENTS

	Page
SUMMARY	1
INTRODUCTION	1
GENERALIZED EQUATIONS	2
APPLICATION TO ONE-DIMENSIONAL DENSITY DISTRIBUTION	5
Theoretical Limitations	8
Apparent-ray-trace crossing	9
Series convergence	10
Applicability criterion	10
Extended or misalined light source	10
Light-source geometry	11
Test-section windows	11
Analytical Verification	12
Experimental Verification	13
Comparison with Other Analyses	13
APPENDIXES	
A - SYMBOLS	15
B - GENERALIZED FRINGE-SHIFT EQUATION	19
C - DERIVATION OF EVALUATION EQUATIONS ASSOCIATED WITH A ONE-DIMENSIONAL DISTRIBUTION $\rho(y)$	20
Light Path	20
Optical Distortion	24
Fringe Shift	25
D - RELATION BETWEEN MEASURED AND DISTORTIONLESS FRINGE-SHIFT PROFILES ASSOCIATED WITH A ONE-DIMENSIONAL DISTRIBUTION $\rho(y)$	28
E - LIMITATIONS OF TWO-TERM EVALUATION EQUATIONS ASSOCIATED WITH A ONE-DIMENSIONAL DISTRIBUTION $\rho(y)$	31
Apparent-ray-trace crossing	31
Series convergence	33
Applicability criterion	34
Test-section windows	35
F - THREE-TERM EVALUATION EQUATIONS ASSOCIATED WITH A ONE-DIMENSIONAL DISTRIBUTION $\rho(y)$	37
G - EQUATIONS FOR CALCULATING PROFILE N_D ASSOCIATED WITH A HYPOTHETICAL EXPONENTIAL-DENSITY PROFILE	39
H - EXPERIMENTAL VERIFICATION OF REFRACTION EFFECT	43
REFERENCES	45

3197

NATIONAL ADVISORY COMMITTEE FOR AERONAUTICS

TECHNICAL NOTE 3340

GENERALIZATION OF GAS-FLOW-INTERFEROMETRY THEORY AND INTERFEROGRAM EVALUATION EQUATIONS FOR ONE-DIMENSIONAL DENSITY FIELDS

By Walton L. Howes and Donald R. Buchele

3197

SUMMARY

Interferogram evaluation equations for calculating one-dimensional density distributions from optical-interference records are derived from generalized equations. The resulting evaluation equations are applicable for any plane of focus. Assumptions involved in the derivations are more general than heretofore and permit determination of limitations and systematic errors of the evaluation equations. Errors caused by an extended or misalined light source and by test-section windows are found to be negligible when the extension or misalinement is small compared with the focal length of the collimating lens. A criterion for applicability of the evaluation equations is established, and a criterion for avoiding apparent-ray-trace crossing is derived.

The proposed evaluation equations and procedures are compared with previous results and are tested in a hypothetical and an experimental situation involving known density distributions.

INTRODUCTION

Zehnder-Mach interferometers have been employed in recent years for quantitative studies of various aerodynamic and thermodynamic phenomena (refs. 1 to 6), particularly boundary layers. The optical-interference method possesses the important advantages of permitting instantaneous quantitative recording of the entire phenomenon without disturbing it. However, because the interference method is integrative, it is presently restricted to certain quantitative applications by mathematical limitations that are primarily attributable to the geometry of the phenomenon and to optical refraction.

Practical interferogram evaluation equations for one-dimensional density fields, where the density gradient is essentially perpendicular to the incident light path, have been proposed in references 7 to 11 and include the effects of optical refraction. In references 7 to 10 a

simple evaluation procedure is developed; however, this procedure in its most general form necessitates a "shifting" procedure, becomes invalid in the presence of apparent-ray-trace crossing, and may not apply in the immediate vicinity of surfaces. In the present report the analysis given in reference 11 is generalized and modified in an attempt to eliminate the preceding difficulties and to determine the importance of various systematic errors.

GENERALIZED EQUATIONS

3197

General functional relations giving the refractive-index distribution as a function of measurable quantities and considering a laterally extended light source are derived. For subsequent simplicity, the following assumptions are made:

(1) The interferometer optical system is perfect.

(2) The light incident at the test section, which contains the phenomenon to be studied, is perfectly collimated.

(3) The refractive index of the medium to be studied is very nearly unity.

(a) The test medium possesses no internal space discontinuities of refractive index, such as shock waves, in the region of interest.

(b) The test medium is bounded by plane discontinuities, such as wind-tunnel windows, perpendicular to the optical axis of the interferometer optical system.

(4) All other media traversed by the light possess a constant refractive index.

References 9 and 11 have shown that the pertinent effects of wind-tunnel windows are insignificant for the case of an axial point-light-source. It will presently be shown that window effects are also essentially negligible with respect to light emitted from off-axis source points. Hence, the effects of windows bounding the test section will be disregarded temporarily in the subsequent analysis.

The important optical quantities involved in evaluating an unknown density field from an interferogram are: fringe shifts, which denote observed changes of phase and order of interference associated with density changes at fixed points in the field; and, a form of optical distortion (very similar to a mirage) that results from apparent shifts of location of points in the field.

In order to express fringe shifts and distortions as functions of measurable quantities, the light path must be known. Light-ray traces in an optical medium follow Fermat's principle, namely,

$$\psi = c \int dt = \int \mu \, ds = \text{extremum} \tag{1}$$

which defines an optical-path length ψ (all symbols are defined in appendix A), where c is the velocity of light in vacuum, t is the time required for the light to traverse distances measured along the light paths, and μ is the refractive index of the medium. Fringe shifts N are defined by

$$N = (\bar{\psi}_1 - \bar{\psi}_2)/\lambda \tag{2}$$

where λ denotes a specific wave length of light, and optical lengths $\bar{\psi}_1$ and $\bar{\psi}_2$ are associated with coherent light waves and are measured from the light source to the plane at which interference is recorded. Two or more light waves are coherent and, hence, may be observed to interfere at the interferometer image plane when any pair of ray traces associated with the waves proceeds from the same light-source point and intercepts the same image point.

A few representative ray traces throughout an interferometer optical system are shown in figure 1. Interference at a given image point may be represented generally in terms of one ray trace contained in the test beam (trace 1), which traverses the test section, in conjunction with a second ray trace contained in the reference beam (trace 2), which circumvents the test section. However, it can be easily demonstrated (ref. 8) that those fringe shifts which are of practical interest may be expressed in terms of ray traces in the test beam alone. Thus, the word "reference" will henceforth refer to reference conditions pertaining to the test beam. The fringe shifts of immediate practical interest are:

(1) N_c, associated with the refractive index change μ_a to μ_∞ within the test section, where the subscript a refers to atmosphere external to the test section, and the subscript ∞ refers to ambient conditions within the test section

(2) N, associated with the refractive index change μ_∞ to μ within the test section, where generally $\mu = \mu(x,y,z)$ and x,y,z are cartesian space coordinates

Let the x,y,z coordinate system be a right-handed system, as defined in figure 1. Then, including fringe shifts contributed by off-axis points in the light source, it is shown in appendix B that

3197

CM-1 back

$$N = \frac{1}{\lambda}\left\{\int_0^L \mu\left[1 + \left(\frac{dx}{dz}\right)^2 + \left(\frac{dy}{dz}\right)^2\right]^{1/2} dz - \mu_\infty L \sec \varphi_r - \mu_a D \sin \Phi(-1) + \mu_a KL\left[\sec \varphi_r(+1) - \sec \Phi(+1)\right]\right\} \tag{3}$$

where, as shown in figure 2, L is the test-section span, Φ is the angle that a particular ray trace makes with the z-axis, D is the optical distortion which has been defined previously in reference 11 and will subsequently be discussed, and K is a fraction of the test-section span defined by

$$K = 1 - \frac{z_R}{L} \tag{4}$$

where the real object-plane $z = z_R$ is the real locus of objects imaged at the selected image plane. All geometrical quantities in equation (3), except those quantities bearing the subscript r, are referred to ray traces that traverse the field μ. The subscript r refers to reference traces that traverse the field μ_∞. Quantities denoted (-1) or (+1) are referred to the medium immediately preceding or succeeding the test section (atmosphere, as a result of the present assumptions), respectively. Equation (3) represents a set of equations for each point of the interferogram, one equation corresponding to each pertinent pair of ray traces which intercepts a given image point.

If μ_a replaces μ_∞ as a reference and μ reduces to the constant value μ_∞, then equation (3) reduces to

$$N_c = \frac{1}{\lambda}\left[\mu_\infty L \sec \Phi - \mu_a L \sec \varphi_r - \mu_a D \sin \Phi\ (-1)\right] \tag{3a}$$

which is most commonly applied in the paraxial form

$$N_c = \frac{1}{\lambda}(\mu_\infty - \mu_a) L \tag{3b}$$

associated with an axial point-light source (ref. 12).

Distortion of the locations of conjugate points can be derived by inspection of figure 2. Thus,

$$D = \pm\left[(l_L - H)^2 + 2l_L H (1 - \cos u)\right]^{1/2} \tag{5}$$

where

3197

$$l_L = \pm\left\{(l - l_r)^2 + 2ll_r\left[1 - |\cos v\ (+1)|\right]\right\}^{1/2} \tag{5a}$$

$$l = KL\,|\sec \varphi(+1)| \tag{5b}$$

$$l_r = KL\,|\sec \varphi_r(+1)| \tag{5c}$$

and v is the angle of refraction, H is the refraction displacement perpendicular to the z-axis at plane $z = L$, and u is the angle formed by the intersections of a trace through the field μ, its unrefracted extension from plane $z = 0$, and the associated reference trace through the field μ_∞ at, and in, the plane $z = L$.

Equations (3) and (5) are useful for starting the derivation of interferogram-evaluation equations for particular refractive-index-field geometries and for investigating effects of extended or off-axis light sources.

APPLICATION TO ONE-DIMENSIONAL DENSITY DISTRIBUTION

Because of mathematical complications, only the following cases have been considered:

(1) μ = constant

(2) $\mu = \mu(y)$ or $\mu(x)$

(3) $\mu = \mu(r)$ $\quad (r^2 = x^2 + y^2)$ or

$\mu = \mu(R)$ $\quad (R^2 = x^2 + y^2 + z^2)$

An evaluation equation for case (1) is supplied, in general, by equation (3a) and for the particular case of the axial point-light-source by equation (3b). Evaluation methods for case (2) have been described in references 7 to 11. Evaluation methods for case (3) have been described extensively in several papers including references 1, 13, 14, and 15. The present report is concerned with case (2) in which μ is a function of a single cartesian coordinate, say y, which is perpendicular to the optical axis. (The density ρ is related to the refractive index by the Dale-Gladstone formula

$$\mu = 1 + k\rho$$

where k, the specific refractivity, is a constant for any given wave length.) However, it is noteworthy that equations (3) and (5) also reduce to the standard starting equations employed for evaluating axially symmetric distributions $\mu(r)$ (refs. 1, 13, 14, and 15).

3197

Evaluation equations for density distributions of the form $\rho(y)$ are derived in series form in appendixes C and D by utilizing equations (3) and (5). For simplicity the evaluation equations are expressed in terms of the object-space coordinate y, which is related to the corresponding image-space coordinate y' by

$$y' = -my$$

where m is the lateral magnification introduced by the camera lens. Also, the distribution $\rho(y)$ is evaluated in terms of the density ratio ρ^*, where at a given ordinate value y_0

$$\rho^* = \frac{\rho(y_0)}{\rho_\infty}$$

The present evaluation equations are based, whenever possible, upon simplifying assumptions involving the independent variables of an experiment, for example, refractive index, geometry of the phenomenon, or geometry of the experimental apparatus, rather than, for example, the light path. The principal additional assumptions are as follows:

(1) The refractive index μ is a monotonic function of y along any given ray trace.

(2) The function μ is representable along any given ray trace by the power series $\mu_\eta = \sum b_\nu \eta^\nu$, where the cartesian coordinate η is defined by $\eta = |y - y_0|$. This permits simplification and extension of the analysis to decreasing, as well as increasing, functions $\mu(y)$. Approximations are denoted one-term, two-term, ... according to the number of terms of the series $\sum b_\nu \eta^\nu$ which is utilized.

(3) Ray traces are representable by the power series $\eta = \sum c_\sigma \zeta^\sigma$ in the interval $o \leqq \zeta \leqq L$, where $\zeta \equiv z$.

According to the preceding assumptions, one- and two-term approximations are associated with the following additional assumptions:

One-term approximation:

(a) Along any given ray trace, μ = constant.

(b) The ray traces are straight lines through the test section.

(c) The measured fringe-shift profile is always distortionless.

3197

(d) The measured fringe-shift profile is a step function of y or a constant for all values of y.

Two-term approximation:

(a) Along any given ray trace μ is a linear function of y.

(b) The ray traces are parabolas within the test section.

(c) The measured fringe-shift profile is distortionless when the selected object plane corresponds to the midspan plane of the test section.

3197

One- and two-term approximations and the corresponding evaluation procedures associated with an axial point-light-source are as follows:

One-term approximation: $\mu_\eta = b_0$

(a) $\rho^* = 1 + N \frac{\lambda}{k\rho_\infty L}$

Two-term approximation: $\mu_\eta = b_0 + b_1\eta$

(a) $\rho^* = 1 + \frac{1}{k\rho_\infty}\left[N \frac{\lambda}{L} - \frac{1}{6}(2 - 3K)\, b_1^2 L^2\right]$

(b) $y \equiv y_0 = y_D - D$

(c) $D = \pm \frac{1}{2}(1 - 2K)\, b_1 L^2$ (see footnote)

(d) $b_1 = \left|\frac{dN}{dy_D}\right| \frac{\lambda}{L}$ $\left(\text{Incidentally, } b_1 = k\left|\left(\frac{d\rho}{dy}\right)_{y_0}\right|, \text{ also.}\right)$

Evaluation procedure:

(a) Plot N as a function of y_D graphically from measured data.

(b) At each datum point measure the slope of the resulting profile N_D.

(c) For each datum point compute b_1, then ρ^*, D, and y_0 (if necessary). The density ratio ρ^* as a function of y represents the desired profile.

The convention + or - is associated with $\mu(y)$ increasing or decreasing, respectively.

Although, when $K = 1/2$, the preceding one- and two-term evaluation equations are identical to the corresponding results indicated in reference 11, important differences are made evident by the derivations, namely:

(1) The present evaluation equations apply for any value of K and permit direct calculation of ρ^* without recourse to a shifting procedure (refs. 8 to 10).

(2) The additional assumption $dD/dy = 0$ (stated somewhat incompletely as $D = 0$ in ref. 11) is unnecessary (but instead follows as a direct result of the two-term assumption), so that mention in reference 11 of an iteration process for eliminating residual distortion is inconsistent with respect to the primary analysis.

3197

By relating derivatives of the measured fringe-shift profile to derivatives of the corresponding hypothetical distortionless profile and then to coefficients b_ν, it follows from the derivations in appendixes C and D that, as a result of the two-term approximation, $dN/dy_D = dN/dy$ because $dD/dy = 0$; that is, the slope of the measured fringe-shift profile at $y = y_D$ has the same value as that of the corresponding hypothetical distortionless-fringe-shift profile at $y = y_0$. Thus, correct values of the coefficient b_1 are presumably determinable from the measured fringe-shift profile associated with any value of K, and, hence, the present equations apply for any value of K.

Theoretical Limitations

The analysis described in appendixes C and D can be used to obtain theoretical information concerning limitations of the interferometric method and the preceding evaluation equations and concerning the importance of certain other systematic errors. In the succeeding paragraphs the following items are considered:

(1) Establishment of a criterion for minimizing apparent-ray-trace crossing

(2) Series convergence and the calculation of remainders associated with the finite approximations

(3) Establishment of a criterion for the applicability of the proposed evaluation equations

(4) Estimation of the importance of lateral extension or misalinement of the light source

(5) Determination of desirable light-source geometries

(6) Estimation of the effect of test-section windows with respect to off-axis light-source points

Apparent-ray-trace crossing. - Apparent-ray-trace crossing, which has been noted in references 9 and 10, occurs when the relative magnitudes of the initial ordinates y_0 and corresponding apparent ordinates y_D associated with any pair of refracted ray traces are reversed (as in the case of an inverted mirage). Two cases of apparent-ray-trace crossing are illustrated in figure 3. In figure 3(a) "crossing" prevails throughout the interval for which

$$\frac{1}{2} \geqq K \geqq -\infty$$

whereas in figure 3(b) crossing occurs throughout the interval for which

$$\frac{1}{2} \leqq K \leqq \infty$$

It is demonstrated in appendix E that crossing occurs whenever

$$\left|\frac{\Delta D}{\Delta y}\right| \geqq 1$$

Regions of an interferogram that are associated with crossing exhibit multiple imagery in that records of two or more regions of the field $\rho(y)$ are superimposed and interrelated. Such regions probably cannot be evaluated unless one trace of each of the crossed pairs is prevented from reaching the final image plane. Unfortunately, the existence of crossing may not be apparent from the interferogram.

The possibility of crossing can generally be alleviated by the proper choice of K. It is shown in appendix E that, for arbitrary functions $\rho(y)$, apparent-ray-trace crossing is least likely to occur when $K \approx 1/2$ because dD/dy is essentially zero when $K = 1/2$. A criterion for avoiding apparent-ray-trace crossing is also derived in appendix E as follows: The existence of apparent-ray-trace crossing is unlikely when the inequality

$$\left| \pm \frac{1}{2}(1 - 2K)\, k \overline{\frac{d^2\rho}{dy^2}}\, L^2 + \frac{1}{24}(1 - 4K) \left(k \overline{\frac{d^2\rho}{dy^2}}\, L^2 \right)^2 \right| \leqq 1$$

is satisfied. The inequality may be satisfied by properly selecting K if information regarding the expected extreme value of $d^2\rho/dy^2$ is available prior to the experiment.

3179 CM-2

Series convergence. - It has been shown in reference 9 that, if the series expansions for μ and η converge, then the resulting power series for ρ^* and D also converge. The introduction of a laterally extended light source still yields a convergent series, but differentiation of series may not always yield a convergent series. In an arbitrary experiment the existence of convergence is not assured, although it would appear that the power series for ρ^* and D are usually convergent or, at least, asymptotic because the one-term expression for ρ^* has always been found to yield results which are in reasonably good agreement with predicted physical values of ρ^*.

The remainders associated with the one- and two-term approximations of ρ^* and D are given in appendix E, where remainders associated with the two-term approximation depend upon the three-term approximation which is derived in appendix F.

Applicability criterion. - A criterion for the applicability of the two-term approximation is derived in appendix E. It is shown that the two-term approximation is likely to be valid for at least those regions of the field for which the second derivative of the measured fringe-shift profile satisfies the inequalities

$$\frac{-8}{\lambda L} < \pm \frac{d^2N}{dy_D^2} < \frac{14}{\lambda L} \quad \text{when} \quad K = \frac{1}{3}$$

$$\frac{-1.7}{\lambda L} < \pm \frac{d^2N}{dy_D^2} < \frac{1.6}{\lambda L} \quad \text{when} \quad K = \frac{1}{2}$$

$$\frac{-0.8}{\lambda L} < \pm \frac{d^2N}{dy_D^2} < \frac{0.5}{\lambda L} \quad \text{when} \quad K = 1$$

Calculation of ρ^* and D up to and including the two-term approximation is practical. Higher-order approximations are excessively complicated and are limited by the inaccuracy of measuring higher-order derivatives of N. Also, no practical situation has yet been encountered in which the additional terms involved in the three-term approximation are appreciable.

Extended or misalined light source. - Estimation of the importance of off-axis light-source points resulting from lateral extension or misalinement of the light source can be made by inspecting the equations for ρ^* and D which are derived in appendix C. Thus, if p and q represent coordinates of light-source points in a plane perpendicular to the optical axis such that

3197

$$p = - x + \text{constant} \qquad \left|\frac{dp}{dx}\right| \equiv 1$$

$$q = - y + \text{constant} \qquad \left|\frac{dq}{dy}\right| \equiv 1$$

where the origin $(p,q) \equiv (0,0)$ lies on the optical axis, then the effects of off-axis source points are expressed by

$$\delta\rho^* \approx 0 \quad \text{if} \quad \left(\frac{p}{f}\right)^2, \left(\frac{q}{f}\right)^2 << 1$$

and

$$\delta D \approx 0 \quad \text{if} \quad \left(\frac{p}{f}\right)^2, \left|\frac{q}{f}\right| << 1$$

where δ denotes the variation of value of the associated quantity from its value when the light source consists of an axial point, and f is the focal length of the collimating lens. The pertinent quantities are indicated in figure 4. Experimental evidence, which qualitatively confirms the preceding conclusion, is presented in reference 8.

Light-source geometry. - It is found by inspecting the series expansions for ρ^* and D in appendix C that, from the standpoint of evaluation-equation simplicity, light-source geometries in order of decreasing desirability are:

(1) Axial point

(2) Narrow slit along p-axis

(3) Narrow slit along q-axis

(4) Extension in p,q-plane

Test-section windows. - For simplicity, the effects of test-section windows upon N and D were disregarded in the preceding analysis. It is shown in appendix E that window effects are negligible when

$$\left(\frac{q}{f}\right)^2 << 1$$

and

$$\left(\frac{p}{f}\right)^2 << 1$$

3197 CM-2 back

Analytical Verification

The validity of proposed evaluation procedures can be investigated and their limitations illustrated by calculating exactly the profile N_D associated with an assumed hypothetical profile $\rho(y)$ and then by attempting to recalculate $\rho^*(y)$ from the proposed evaluation equations and the computed profile N_D. However, the equations for computing N_D must be assumed correct and exact, or nearly so. Otherwise the evaluation equations may effect an excellent reproduction of the assumed profile $\rho^*(y)$ although they are incorrect, as was the case in reference 16

3197

The present evaluation equations were tested by assuming an exponential profile $\rho(y)$. The profiles N_D were calculated accurately and the recomputed profiles $\rho^*(y)$ were calculated to one-, two-, and three-term approximations for three values of K, namely $K = 1/3$, $1/2$, and 1 and for two values of L, namely $L = 1.8$ and 3.6 inches. The equations for calculating N_D are given in appendix G. The recomputed profiles $\rho^*(y)$ for $L = 1.8$ and 3.6 inches are presented in figures 5 and 6, respectively. The two-term profiles for $K = 1/2$ and $L = 1.8$ and 3.6 inches are compared in figures 7(a) and (b), respectively, with the corresponding profiles obtained by using the Wachtell-DeFrate method (refs. 7 to 10).

A value of the exponential coefficient a (appendix G) was selected that would introduce strong nonlinearities in the profile $\rho(y)$ and hence permit illustration of limitations of the interferometric analysis and evaluation equations.

For $L = 1.8$ inches, the two- and three-term approximations yielded recomputed profiles $\rho^*(y)$ that are in excellent agreement with the assumed profile $\rho^*(y)$ for all values of K (as suggested in the previous discussion) and represent definite improvements over the results of the one-term approximation. It is apparent from figure 7(a) that the two-term approximation for $K = 1/2$ permits evaluation closer to the surface ($y = 0$) than does the Wachtell-DeFrate method. In particular, $\rho(y)$ is only determinable for

$$y \geqq 0.0032 \text{ inch for } K = 1/3 \text{ (method of refs. 7 to 10)}$$

$$y \geqq 0.0012 \text{ inch for } K = 1/2 \text{ (method of present report)}$$

For $K = 1/2$ and 1 the maximum absolute magnitudes of d^2N/dy_D^2 slightly exceed the values set by the applicability criterion, but the agreement of the two-term result with the assumed profile $\rho^*(y)$ is still very good.

The ratios of successive terms of the series expansions for ρ^* and D are proportional to L. Therefore, as L is increased, higher-order terms increase in relative importance. For L = 3.6 inches, the two-term approximation represents an improvement over the one-term approximation, and the profiles for all values of K are in agreement; however, because of the increased value of L the y interval of good agreement with the assumed profile $\rho^*(y)$ is considerably reduced. In particular, the recomputed profile $\rho^*(y)$ for $K = 1/3$ is strongly affected by apparent-ray-trace crossing and the recomputed profile $\rho^*(y)$ for $K = 1/2$ is slightly affected, as is apparent from figure 8. However, distortion is smallest when $K = 1/2$ and is an absolute over-all minimum for some plane in the interval $1/2 < K < 1$, as is $|dD/dy|$. For all values of K, the maximum absolute values of d^2N/dy_D^2 exceed the values set by the applicability criterion. However, the profiles $\rho^*(y)$ recomputed according to the two-term approximation do not begin to deviate appreciably from the assumed profile until the criterion has been definitely violated. Thus, it may be tentatively surmised that the applicability criterion is somewhat conservative. The three-term profile $\rho^*(y)$ is strongly affected by the preceding difficulties and is less useful than the profile obtained from the two-term calculation. According to figure 7(b) the Wachtell-DeFrate result is again limited to a smaller y interval than the present two-term result.

3197

Experimental Verification

In order to verify conclusively the existence and magnitude of the optical-refraction effect, an experiment was devised for measuring the effect and confirming the refraction terms associated with the two-term approximation of ρ^* and D. Good agreement was obtained between theory and experiment. Details and results of the experiment are discussed in appendix H.

Comparison with Other Analyses

Objections to analyses presented in references 16 and 17 have been discussed in references 9 and 10. Objections to the analysis in reference 11 have already been discussed in the present report.

Results given by the two-term equation derived independently by Wachtell and DeFrate (refs. 7 to 10) are equivalent to those given by the present one-term equation when $K = 1/3$. The former equation may be readily derived from the present two-term equation. For any other selected value of K, Wachtell in references 9 and 10 proposed a "shifting" procedure by which an uncorrected density profile is computed and then corrected by means of shifting equations to give the

profile associated with $K = 1/3$. However, if apparent-ray-trace crossing occurs when $K = 1/3$, then the entire method fails because the density profile must be corrected to $K = 1/3$. For $K = 1/3$,

$$D = \pm \frac{b_1 L^2}{6}$$

so that a ray trace that satisfies $y = 0$ at $z = 0$, where $y = 0$ represents the surface of a model, will generally appear at $y = D \neq 0$ (ref. 8). Thus, the Wachtell-DeFrate method can only be used to evaluate ρ^* in the immediate vicinity of a surface when $(d\rho/dy)_0 = 0$.

3197

By comparison, failure of the present method resulting from apparent-ray-trace crossing should not occur because the corrected density profile is associated with the selected value of K, rather than with $K = 1/3$, specifically. Generally, a value of K can be chosen for which crossing is absent. Moreover, the computed distortion is zero if $K = 1/2$. However, slopes dN/dy_D must be measured, and a refraction term must be computed in calculating ρ^*. On the other hand, $\rho^*(y)$ can be computed for any other selected value of K without recourse to a shifting procedure if D is computed. The total amount of computation is equivalent to that of the Wachtell-DeFrate method with shifting.

In reference 8 an iteration procedure is proposed which presumably can be applied when $\rho(y)$ is extremely nonlinear and when there is no apparent-ray-trace crossing. However, the iteration method in comparison with the preceding approximation methods necessitates an excessive amount of computation and some degree of guesswork.

Lewis Flight Propulsion Laboratory
National Advisory Committee for Aeronautics
Cleveland, Ohio, November 19, 1954

APPENDIX A

SYMBOLS

The following symbols are used in this report:

a	exponential refractive-index-distribution coefficient
b_ν	refractive-index coefficients
$b_{\nu,1}, b_{\nu,2}$	refractive-index coefficient; first and second approximations, respectively
C	constant
c	velocity of light
c_σ	light-path coefficients
c_σ^*	light-path coefficients
$c_{\sigma,\nu}$	fringe-shift coefficients
D	optical distortion
e	exponential
f	focal length of collimating lens
H	refraction displacements of ray traces in and at plane $z = L$
K	fraction of test-section span, $K = 1 - \frac{z_R}{L}$
$K_{\tau,\sigma}$	constant, $K_{\tau,\sigma} = \tau - \sigma K$
k	specific refractivity
L	test-section span
l_L, l, l_r	lengths given by equations (5a), (5b), and (5c), respectively (fig. 2)
m	lateral magnification
N	interference-fringe shift

3197

3197

N_O	function representing hypothetical distortion-free interference-fringe-shift profile
N_D	function representing measured (distorted) interference-fringe-shift profile
n	integer
p	light-source coordinate parallel to x-coordinate
q	light-source coordinate parallel to y-coordinate
R	radius in spherical coordinates
R	remainder
r	radius in cylindrical coordinates
s	length measured along ray trace
T	absolute temperature
t	time
t	window thickness
t	quantity defined in appendix G
u	angle formed by intersection of refracted-ray trace, its unrefracted extension from plane $z = 0$, and its associated reference trace at, and in, plane $z = L$ (fig. 2)
v	refraction angle of refracted ray-trace (fig. 2)
x,y	cartesian coordinates perpendicular to optical axis
y_O	y-coordinate value of ray trace at plane $z = 0$; y-coordinate values associated with profile N_O
y_D	apparent y-coordinate value of source of ray trace; y-coordinate values associated with profile N_D
Z(t)	axial separation of real- and apparent-object plane
z	optical axis
z_R	real-object plane

α	projected angle in xy- or $\xi\eta$-plane
β	projected angle in yz- or $\eta\zeta$-plane
γ	projected angle in xz- or $\xi\zeta$-plane
Δ	increment
δ	variation or change
ζ	ray-trace coordinate parallel to optical axis
η	ray-trace coordinate perpendicual to optical axis
$\varkappa_1,\varkappa_2$	coefficients
λ	wave length of light
μ	refractive index
ν	integer
ξ	ray-trace coordinate perpendicular to optical axis
ρ	density
ρ^*	density ratio, $\rho^* = \rho(y_0)/\rho_\infty$
σ,τ	integers
φ	angle formed by ray trace and optical axis
ψ	optical-path length
(-2),(-1)	refers to mediums preceding test section
(+1),(+2)	refers to mediums succeeding test section

Subscripts:

A	refers to lower surface of upper block in hot-plate model
a	atmosphere
c	refers to change of refractive index within test section from that of the external atmosphere to some other constant value

3197
CM-3

3197

g	window
r	reference ray trace
w	value at wall, or surface
m,n,ν,σ,τ	integers
∞	refers to ambient conditions within test section

Superscript:

'	refers to image space associated with camera lens
$\bar{}$	maximum absolute value

3197

CM-3 back

APPENDIX B

GENERALIZED FRINGE-SHIFT EQUATION

In general, the interference fringe shift measured at a given image point is represented by equation (2), namely

$$N = (\bar{\psi}_1 - \bar{\psi}_2)/\lambda \tag{2}$$

The quantities $\bar{\psi}_1$ and $\bar{\psi}_2$ are determined from associated ray traces whose paths in any given optical medium are found from the first-order partial differential equation (ref. 18)

$$\left(\frac{\partial \psi}{\partial x}\right)^2 + \left(\frac{\partial \psi}{\partial y}\right)^2 + \left(\frac{\partial \psi}{\partial z}\right)^2 = \mu^2 \tag{B1}$$

Equation (B1) is the solution of the variation problem indicated by equation (1), where $\mu = \mu(x,y,z)$ may be an arbitrary function of the cartesian coordinates x, y, z.

If $\bar{\psi}_1$ and $\bar{\psi}_2$ are associated with ray traces which traverse the fields μ and μ_∞, respectively, then $\Delta\psi = \bar{\psi}_1 - \bar{\psi}_2$ is determined by ray traces 1 and 2 in figures 1 and 2; these traces satisfy the requirements for interference because they are parallel in the space preceding the test section. It is shown in references 7, 8, and 11 that $\Delta\psi$ is determined entirely in the interval bounded by the plane wavefronts in the medium (-1), which immediately preceeds the test section, and by the effective plane, or spherical, wavefronts determined by traces 1 and 2 in the medium (+1). Thus, N may be expressed by inspection in terms of the geometrical quantities shown in figure 2. The result is equation (3), in which the first term on the right-hand side is attributed to the trace through the field μ, the second term to the trace through the field μ_∞, the third term to obliquity of traces in medium (-1), and the last term to obliquity of traces in medium (+1) plus refraction.

APPENDIX C

DERIVATION OF EVALUATION EQUATIONS ASSOCIATED WITH A ONE-DIMENSIONAL DISTRIBUTION $\rho(y)$

Light Path

Light ray traces are determined by

$$\left(\frac{\partial\psi}{\partial x}\right)^2 + \left(\frac{\partial\psi}{\partial y}\right)^2 + \left(\frac{\partial\psi}{\partial z}\right)^2 = \mu^2 \tag{B1}$$

For a function $\mu = \mu(y)$, equation (B1) possesses a solution of the form

$$\psi(x,y,z) = \psi_1(x) + \psi_2(y) + \psi_3(z)$$

namely

$$\psi = \pm C_1(x - x_0) \pm \int_{y_0}^{y} \sqrt{\mu^2 - C_2^2}\, dy \pm C_3(z - z_0)$$

where

$$C_2^2 = C_1^2 + C_3^2$$

are constants. Applying Jacobi's theorem (ref. 18) reduces the solution for ψ to solutions for the ray traces, namely

$$\frac{dy}{dz} = \pm \frac{1}{C_3}\sqrt{\mu^2 - C_2^2} = \tan\beta$$

$$\frac{dy}{dx} = \pm \frac{1}{C_1}\sqrt{\mu^2 - C_2^2} = \tan\alpha$$

Initially, when

$$x = x_0 \qquad y = y_0 \qquad z = z_0 = 0$$

then

$$\alpha = \alpha(x_0) \qquad \beta = \beta(0)$$

3197

and the constants C_1 and C_3 are given by

$$C_1^2 = \frac{\left[\mu(y_0)\right]^2 \tan^2 \gamma(0)}{1 + \tan^2 \beta(0) + \tan^2 \gamma(0)}$$

$$C_3^2 = \frac{\left[\mu(y_0)\right]^2}{1 + \tan^2 \beta(0) + \tan^2 \gamma(0)}$$

5197

where

$$\frac{dx}{dz} = \tan \gamma$$

Thus, the ray traces are given by

$$1 + \left(\frac{dy}{dz}\right)^2 + \tan^2 \gamma(0) = \left[\frac{\mu(y)}{\mu(y_0)}\right]^2 \sec^2 \varphi(0) \qquad (C1)$$

where

$$\sec^2 \varphi(0) = 1 + \tan^2 \beta(0) + \tan^2 \gamma(0)$$

and

$$\frac{dy}{dx} = \text{constant}$$

Equation (C1), which applies when $\mu(y)$ is an increasing function, can be extended to include cases where $\mu(y)$ is a decreasing function and, also, ultimately to lead to simpler evaluation equations by introducing auxiliary, floating, coordinates ξ, η, ζ defined by

$$\xi = |x - x_0| \qquad \left|\frac{d\xi}{dx}\right| \equiv 1$$

$$\eta = |y - y_0|$$

$$\zeta = z \qquad \left|\frac{d\eta}{dy}\right| \equiv 1$$

The coordinates of any given ray trace are then $(\xi,\eta,\zeta) \equiv (0,0,0)$ at $z = 0$. In terms of the new coordinates, μ_η corresponds to $\mu(y)$ and

$$\mu_0 \equiv \mu(y_0) \qquad \alpha_0 \equiv \pm \alpha(x_0) \qquad \beta_0 \equiv \pm \beta(0)$$

$$\gamma_0 \equiv \pm \gamma(0) \qquad \varphi_0 \equiv \pm \varphi(0)$$

Then equation (C1) becomes

$$1 + \left(\frac{d\eta}{d\xi}\right)^2 + \tan^2 \gamma_0 = \left(\frac{\mu_\eta}{\mu_0}\right)^2 \sec^2 \varphi_0 \tag{C1a}$$

If μ_η is rewritten in the form

$$\mu_\eta = \mu_0 + \Delta\mu_\eta \tag{C2}$$

where, for gases,

$$\mu_0 \approx 1 \quad \text{and} \quad \Delta\mu_\eta << 1 \tag{C3}$$

then equation (C1a) reduces to

$$\left(\frac{d\eta}{d\xi}\right)^2 = 2\,\Delta\mu_\eta \sec^2 \varphi_0 + \tan^2 \beta_0 \tag{C1b}$$

where terms in $(\Delta\mu_\eta)^2$ are infinitesimals of higher order as a result of conditions (C3).

Generally $\Delta\mu_\eta$ is not constant. Then μ_η may be represented by the power series

$$\mu_\eta = \sum_{\nu=0}^{\infty} b_\nu \eta^\nu \tag{C4}$$

$$= \sum_{\nu=0}^{\infty} b_\nu |y - y_0|^\nu \tag{C4a}$$

where

$$b_\nu \equiv \frac{1}{\nu!}\left(\frac{d^\nu u}{d\eta^\nu}\right)_0 \equiv \pm \frac{1}{\nu!}\left(\frac{d^\nu u}{dy^\nu}\right)_{y_0} \tag{C5}$$

and

$$\mu_0 \equiv b_0$$

$$\Delta\mu_\eta = \sum_{\nu=1}^{\infty} b_\nu \eta^\nu << 1$$

3197

Also, let the ray traces be represented by the power series

$$\eta = \sum_{\sigma=0}^{\infty} c_\sigma \zeta^\sigma \tag{C6}$$

where

$$c_\sigma \equiv \frac{1}{\sigma!}\left(\frac{d^\sigma \eta}{d\zeta^\sigma}\right)_0 \equiv \pm \frac{1}{\sigma!}\left(\frac{d^\sigma y}{dz^\sigma}\right)_0 \tag{C7}$$

3197

Utilizing the assumed series (C4) and (C6) results in the following solution of equation (C1b):

$$\eta = \tan \beta_0 \sum_{\sigma=1,3,5,\ldots}^{\infty} c_\sigma^* \zeta^\sigma \sec^{\sigma-1}(\varphi_0) + \sum_{\sigma=2,4,6,\ldots}^{\infty} c_\sigma^* \zeta^\sigma \sec^\sigma \varphi_0 \tag{C8}$$

where the coefficients c_σ^* are functions of the coefficients b_ν; namely

$$\begin{aligned} c_1^* &= 1 & c_3^* &= \frac{1}{3} b_2 & &\ldots \\ c_2^* &= \frac{1}{2} b_1 & c_4^* &= \frac{1}{12} b_1 b_2 & &\ldots \end{aligned} \tag{C9}$$

and the coefficients c_σ are given by

$$c_0 = 0$$

because $\eta = 0$ at $\zeta = 0$, and

$$c_\sigma = \begin{cases} c_\sigma^* \tan \beta_0 \sec^{\sigma-1} \varphi_0 & (\sigma \text{ odd}) \\ c_\sigma^* \sec \varphi_0 & (\sigma \text{ even}) \end{cases} \tag{C10}$$

Expressions (C9) are obtained by substituting series (C4) and (C6) in equation (C1b) and equating coefficients of like powers of ζ. Coefficients c_σ^* (σ even) are identical to the coefficients c_σ defined in reference 11 for the case of an axial point-light-source.

Solutions of equation (C1b) for special light-source geometries are readily obtainable from equation (C8):

(1) The identity $(p,q) \equiv (0,0)$ represents an axial-point light source. Then $\beta_0 = \gamma_0 = 0$, and equation (C8) reduces to the ray-trace equation, which was derived in reference 11.

(2) The identity $(p,q) \equiv (p,0)$ represents a narrow slit-light-source parallel to the x-axis. Then $\beta_0 = 0$, and the resulting simplification of equation (C8) is obvious.

(3) The identity $(p,q) \equiv (0,q)$ represents a narrow slit-light-source parallel to the y-axis. Then $\gamma_0 = 0$, and the resulting simplification of equation (C8) is again obvious.

It should be noted that equation (C8) increases in complexity in the order (1), (2), (3) of the preceding light-source geometries.

3197

Optical Distortion

Because the general fringe-shift equation (3) is a function of the optical distortion D, the distortion will be considered first.

According to equation (C1) individual ray traces in the field $\mu(y)$ are refracted in planes. Then, from figure 2,

$$u = 0$$

and equation (5) reduces to

$$D = H - \ell_L$$

However, as seen from figures 9(a) and (b) which depict ray-trace projections in the xz- and yz-planes, respectively,

$$H - D + KL \tan \beta_0 = KL \tan \beta_L$$

where $\beta = \beta_L$ at $\zeta = L$; therefore,

$$D = H - KL (\tan \beta_L - \tan \beta_0) \qquad (C11)$$

By definition, $H = \eta_{\zeta=L}$ and $\tan \beta = d\eta/d\zeta$, so that in series form H is given by series (C8) with ζ replaced by L, and $\tan \beta_L$ is given by the first derivative of series (C8) with ζ replaced by L. Performing the appropriate substitutions in equation (C11) and reducing the resulting expression, the equation for D, expressed in series form, becomes

$$D = \pm\sum_{\sigma=1}^{\infty} K_{1,\sigma} c_\sigma L^\sigma + KL \tan \beta_0 \qquad \text{(C11a)}$$

where, by definition,

$$K_{1,\sigma} = 1 \mp \sigma K$$

The algebraic sign of D has been chosen to be consistent with the coordinate y when D is measured with respect to the distortion-free object point. The resulting sign convention with respect to D is the reverse of that used in reference 11.

When $(p,q) \equiv (0,0)$, equation (C11a) reduces to the distortion equation that was derived in reference 11.

Fringe Shift

When $\mu = \mu(y)$ the integral in equation (3) may be rewritten for subsequent simplicity in terms of μ_η and the coordinates ξ, η, ζ. Then, by successive substitutions

$$\int_0^L \mu_\eta \left[1 + \left(\frac{d\xi}{d\zeta}\right)^2 + \left(\frac{d\eta}{d\zeta}\right)^2\right]^{1/2} d\zeta$$

$$= \int_0^L \mu_\eta \left[1 + \tan^2 \gamma_0 + \left(\frac{d\eta}{d\zeta}\right)^2\right]^{1/2} d\zeta$$

$$= \frac{\sec \varphi_0}{\mu_0} \int_0^L \mu_\eta^2 \, d\zeta$$

$$= \sec \varphi_0 \left(\mu_0 L + 2\int_0^L \Delta\mu_\eta \, d\zeta\right)$$

where terms in $(\Delta\mu_\eta)^2$ are infinitesimals of higher order. Because $\mu_\eta \approx 1$ and test-section windows are disregarded, the following approximations can be made regarding φ, especially when φ is small:

3197

CM-4

$$\sec \varphi_r \approx \sec \varphi_0$$

$$\sin \varphi(-1) \approx \sin \varphi_0$$

$$\sec \varphi_r(+1) \approx \sec \varphi_0$$

$$\sec \varphi(+1) \approx \sec \varphi_L$$

3197

However,

$$\sec \varphi_L = (1 + \tan^2 \beta_L + \tan^2 \gamma_0)^{1/2}$$

$$= \frac{\mu_H}{\mu_0} \sec \varphi_0$$

$$\approx (1 + \Delta\mu_H) \sec \varphi_0$$

Substituting the appropriate preceding quantities in equation (3) yields

$$N = \frac{\sec \varphi_0}{\lambda}\left[(\mu_0 - \mu_\infty) L + 2\int_0^L \Delta\mu_\eta d\zeta - \Delta\mu_H KL - D \sin \varphi_0 \cos \varphi_0\right] \tag{C12}$$

Equation (C12) can be derived in a more exact form by determining the exact expressions for the various angles φ as functions of φ_0 and retaining the multiplicative constants involving μ_∞, μ_a, and μ_0. However, the additional work required is excessive and yields additional terms which are appreciable only when φ is impractically large. When rewritten in series form, equation (C12) becomes

$$N = \frac{\sec \varphi_0}{\lambda}\left[(\mu_0 - \mu_\infty) L + 2\sum_{\nu=1}^{\infty}\sum_{\sigma=1}^{\infty} \frac{b_\nu c_{\sigma,\nu}}{\sigma + 1} L^{\sigma+1} - K\sum_{\nu=1}^{\infty}\sum_{\sigma=1}^{\infty} b_\nu c_{\sigma,\nu} L^{\sigma+1} - \left(\pm\sum_{\sigma=1}^{\infty} K_{1,\sigma} c_\sigma L^\sigma + KL \tan \beta_0\right) \sin \varphi_0 \cos \varphi_0\right] \tag{C12a}$$

where the coefficients $c_{\sigma,\nu}$ are functions of the coefficients c_σ obtained by equating coefficients of like powers of ζ in the expression

$$\sum_{\sigma=1}^{\infty} c_{\sigma,\nu}\zeta^{\sigma} = \left(\sum_{\sigma=1}^{\infty} c_{\sigma}\zeta^{\sigma}\right)^{\nu} \qquad (\nu = 1,2,3,\ldots)$$

The density ratio ρ^* is obtained by solving equation (C12a) for $\mu - \mu_\infty$, utilizing the Dale-Gladstone formula, and dividing both sides of the equation by ρ_∞. Thus,

3197

$$\rho^* = 1 + \frac{1}{k\rho_\infty}\left[N\frac{\lambda}{L \sec \varphi_0} - 2\sum_{\nu=1}^{\infty}\sum_{\sigma=1}^{\infty}\frac{b_\nu c_{\sigma,\nu}}{\sigma+1}L^\sigma + K\sum_{\nu=1}^{\infty}\sum_{\sigma=1}^{\infty} b_\nu c_{\sigma,\nu}L^\sigma + \left(\pm\sum_{\sigma=1}^{\infty} K_{1,\sigma}c_\sigma L^\sigma + KL \tan \beta_0\right)\sin \varphi_0 \cos \varphi_0\right] \qquad (C13)$$

When $(p,q) \equiv (0,0)$, equations (C12a) and (C13) reduce to the corresponding equations for N and ρ^* that were derived in reference 11.

The angle φ_0 is a function of angles β_0 and γ_0. Moreover, β_0 and γ_0 are related to the coordinates (p,q) of the light source. Specifically,

$$\tan \beta_0 = \pm\frac{q}{f}$$
$$\tan \gamma_0 = \pm\frac{p}{f} \qquad (C14)$$

The conclusion stated in the section Extended or misalined light source then results from equations (C11a), (C13), and (C14).

Equations (C11a) and (C13) yield practical evaluation equations for D and ρ^*. However, the coefficients b_ν, c_σ, and $c_{\sigma,\nu}$ must first be expressed as functions of measurable quantities. The coefficients c_σ and $c_{\sigma,\nu}$ are functions of b_ν. Relations permitting the expression of coefficients b_ν as functions of measurable quantities are derived in appendix D.

APPENDIX D

RELATION BETWEEN MEASURED AND DISTORTIONLESS FRINGE-SHIFT PROFILES ASSOCIATED WITH A ONE-DIMENSIONAL DISTRIBUTION $\rho(y)$

The coefficients $c_{\sigma,\nu}$, up to $c_{4,2}$, are given by

$$\begin{aligned} c_{1,1} &= c_1 & c_{1,2} &= 0 \\ c_{2,1} &= c_2 & c_{2,2} &= c_1^2 \\ c_{3,1} &= c_3 & c_{3,2} &= 2c_1c_2 \\ c_{4,1} &= c_4 & c_{4,2} &= c_2^2 + 2c_1c_3 \end{aligned} \tag{D1}$$

Coefficients c_σ are given by equations (C10), and coefficients c_σ^* are given as functions of b_ν by expressions (C9). The coefficients b_ν can be related to measurable space derivatives of the measured fringe-shift profile by considering the relation between space derivatives of the measured fringe-shift profile and derivatives of the corresponding profile that would result if distortion were absent.

Let

(1) $N_O(y)$ denote the fringe-shift profile that would be measured if distortion were absent

(2) $N_D(y)$ denote the observed fringe-shift profile

The y component of separation of the profiles N_O and N_D is the distortion D. The y-coordinate values associated with a given value $N_O = N_D$ are y_O and y_D, respectively, where

$$y_D = y_O + D \tag{D2}$$

and $D = D(y_O)$. In equations (C11a) and (C12a) all quantities, except N, that are variables when associated with a single interferogram are defined with respect to initial values y_O. However, N is associated with values y_D. If the fringe-shift profile is distortionless, then $N_D \equiv N_O$ and is associated with values y_O.

3197

Consider figure 10, which illustrates hypothetical profiles N_D and N_O. In a given fixed interval ΔN, the incremental slopes of the profiles N_O and N_D are, respectively, $(\Delta N/\Delta y)_{y_O}$ and $(\Delta N/\Delta y_D)_{y_D}$. The ratio of the slopes is

$$\left(\frac{\Delta N}{\Delta y}\right)_{y_O}\left(\frac{\Delta y_D}{\Delta N}\right)_{y_D} = \frac{\Delta y_D}{\Delta y}$$

3197

However, it results from equation (D2) that

$$\frac{\Delta y_D}{\Delta y} = 1 + \frac{\Delta D}{\Delta y}$$

Therefore,

$$\left(\frac{\Delta N}{\Delta y_D}\right)_{y_D} = \frac{1}{1 + \frac{\Delta D}{\Delta y}}\left(\frac{\Delta N}{\Delta y}\right)_{y_O}$$

In the limit, as $\Delta y_D \to 0$,

$$\left(\frac{dN}{dy_D}\right)_{y_D} = \frac{1}{1 + \frac{dD}{dy}}\left(\frac{dN}{dy}\right)_{y_O} \tag{D3}$$

Relations between higher derivatives of the fringe-shift profiles may be determined by differentiating equation (D3) with respect to y_D. Thus, the n^{th} derivative is given by the recurrence formula

$$\left(\frac{d^nN}{dy_D^n}\right) = \frac{1}{1 + \frac{dD}{dy}}\frac{d}{dy}\left(\frac{d^{n-1}N}{dy_D^{n-1}}\right) \tag{D4}$$

Derivatives d^nN/dy_D^n are determined from the measured profile N_D, whereas derivatives d^nN/dy^n may be expressed as functions of b_ν by differentiating equation (C12a) with the final distortion-contributed term omitted (because d^nN/dy^n involves no distortion). By direct substitutions equations (D3) and (D4) become, respectively,

$$\left(\frac{dN}{dy_D}\right)_{y_D} = \frac{\sec \varphi_0}{\lambda\left[1 + \sum_{\nu=1}^{\infty} K_{1,\sigma}\left(\frac{dc_\sigma}{dy}\right)_{y_0} L^\sigma\right]}$$

$$\left\{\pm (b_1)_{y_0} L + 2\sum_{\nu=1}^{\infty}\sum_{\sigma=1}^{\infty} \frac{1}{\sigma+1}\left[\frac{d(b_\nu c_{\sigma,\nu})}{dy}\right]_{y_0} L^{\sigma+1} - K\sum_{\nu=1}^{\infty}\sum_{\sigma=1}^{\infty}\left[\frac{d(b_\nu c_{\sigma,\nu})}{dy}\right]_{y_0} L^{\sigma+1}\right\} \tag{D3a}$$

$$\left(\frac{d^n N}{dy_D^n}\right)_{y_D} = \frac{\frac{d}{dy}\left(\frac{d^{n-1}N}{dy_D}\right)_{y_D}}{1 + \sum_{\nu=1}^{\infty} K_{1,\sigma}\left(\frac{dc_\sigma}{dy}\right)_{y_0} L^\sigma} \tag{D4a}$$

which include the effect of off-axis source points. The coefficients b_ν, c_σ, and $c_{\sigma,\nu}$ are functions of y and can be differentiated. However, derivatives of coefficients b_ν are functions of other coefficients $b_{\nu+n}$, namely

$$\frac{d^n b_\nu}{dy^n} \equiv \frac{1}{\nu!}\frac{d^{\nu+n}\mu}{dy^{\nu+n}} \equiv \pm \frac{(\nu+n)!}{\nu!} b_{\nu+n} \tag{D5}$$

as a result of definition (C5). Computations involving a finite number of terms in equations (D3a) and (D4a) and including derivatives of N_D up to the m^{th} derivative must only include coefficients b_ν up to b_m in order to be consistent. Equations (D3a), (D4a), and (D5) then yield expressions for b_ν as functions of measurable derivatives d^nN/dy_D^n.

3197

3197

APPENDIX E

LIMITATIONS OF TWO-TERM EVALUATION EQUATIONS ASSOCIATED WITH A ONE-DIMENSIONAL DISTRIBUTION $\rho(y)$

Apparent-ray-trace crossing. - The condition associated with apparent-ray-trace crossing can be developed by considering two ray traces which possess initial values y_0 and $y_0 + \Delta y_0$, respectively, at $z = 0$, where $|y_0 + \Delta y_0| > |y_0|$. Suppose distortions $D(y_0)$ and $D(y_0 + \Delta y_0)$ are associated with the respective traces. If

$$|y_0 + \Delta y_0 + D(y_0 + \Delta y_0)| > |y_0 + D(y_0)|$$

then "crossing" does not occur because the larger initial and apparent absolute y-values are associated with the same ray trace. However, if

$$|y_0 + \Delta y_0 + D(y_0 + \Delta y_0)| \leqq |y_0 + D(y_0)|$$

then "crossing" occurs because the trace possessing the larger absolute initial value possesses the smaller absolute apparent-value. When the equality is satisfied, the apparent-object points are superimposed. By subtracting y_0 and $D(y_0)$ from both sides of the preceding equation and dividing by Δy_0, the following inequality results:

$$\left|\frac{\Delta D}{\Delta y}\right| \geqq 1 \tag{E1}$$

where

$$\Delta D = D(y_0) - D(y_0 + \Delta y_0)$$

$$\Delta y = y_0 + \Delta y_0 - y_0 = \Delta y_0$$

A practical criterion for avoiding apparent-ray-trace crossing may be derived from inequality (E1). The limiting condition for crossing occurs as $\Delta y \to 0$. Then, inequality (E1) becomes

$$\left|\frac{dD}{dy}\right| \geqq 1$$

The derivative of D can be calculated from equation (C11a). Thus,

$$\left|\frac{dD}{dy}\right| = \left|\sum_{\sigma=1}^{\infty} K_{1,\sigma} \frac{dc_\sigma}{dy} L^\sigma\right|$$

which for the case of an axial point-light-source becomes

$$\left|\frac{dD}{dy}\right| = \left|\sum_{\sigma=2,4,6,\ldots}^{\infty} K_{1,\sigma} \frac{dc_\sigma^*}{dy} L^\sigma\right| \tag{E2}$$

Corresponding to the two-term approximation,

$$\left|\frac{dD}{dy}\right| = 0$$

because equation (E2) is ultimately independent of b_1. However, in the three-term approximation, equation (E2) becomes

$$\left|\frac{dD}{dy}\right| = K_{1,2} b_2 L^2 + \frac{1}{2} K_{1,4} b_2^2 L^4 \tag{E3}$$

With convergence assumed, equation (E3) indicates that $|dD/dy| = 0$ to a first approximation when $K = 1/2$. Also, equation (E3) yields a criterion for avoiding crossing. If the coefficients b_ν $(\nu > 2)$ are assumed to be insignificant, then $|dD/dy| \leqq 1$ when

$$\left|K_{1,2} b_2 L^2 + \frac{1}{6} K_{1,4} b_2^2 L^4\right| \leqq 1 \tag{E4}$$

When apparent-ray-trace crossing exists, the experiment must be repeated using another value of K because none of the evaluation methods apply. Thus, it becomes desirable to express inequality (E4) in terms of quantities that might be estimated before the experiment is performed so that a value of K which will avoid crossing can be selected initially. The most useful result is obtained by expressing b_2 as a function of ρ, namely

$$b_2 = \pm \frac{k}{2} \frac{d^2\rho}{dy^2}$$

which results from the Dale-Gladstone formula and definition (C5). Then, inequality (E4) immediately becomes the crossing-criterion inequality given in the section Apparent-ray-trace crossing.

3197

3197

CM-5

Series convergence. - The series remainders associated with the one-term approximation are given by the additional term contained in the two-term approximations. The remainders associated with the two-term approximations of ρ^* and D are given by the additional terms which are contained in the three-term approximation derived in appendix F. However, because in the third approximation the expression for b_1 becomes modified by the multiplicative factor $\varkappa_1/\varkappa_2$, the additional term involving δb_1 arises in the remainder equations. The remainders associated with the two-term approximation are, therefore, given by

$$\left|R_2(\rho^*)\right| \leq \frac{1}{3k\rho_{\infty}}\left|\left(K_{2,3}b_{1,2}^2L^2\delta b_1 + \frac{1}{5}K_{2,5}\overline{b_{1,3}^2b_2}L^4\right)\right|$$

$$\left|R_2(D)\right| \leq \left|\frac{1}{2}K_{1,2}b_{1,2}L^2\delta b_1 + \frac{1}{12}K_{1,4}\overline{b_{1,3}b_2}L^4\right|$$

where

$$\delta b_1 = \frac{\varkappa_2}{\varkappa_1} - 1$$

$$b_{1,2} = \left|\frac{dN}{dy_D}\right| \frac{\lambda}{L}$$

$$b_{1,3} = \left|\frac{dN}{dy_D}\right| \frac{\varkappa_1}{\varkappa_2} \frac{\lambda}{L}$$

$$b_2 = \pm \frac{d^2N}{dy_D^2} \frac{\varkappa_1^2}{\varkappa_2} \frac{\lambda}{2L}$$

In general,

$$K_{\tau,\sigma} = \tau - \sigma K$$

where τ and σ are integers, and the selected values of the combinations $b_{1,3}^2b_2$ and $b_{1,3}b_2$ correspond to the largest absolute values (denoted by bars) in the interval $y_0 \leq y \leq y_0 + H$ traversed by a given ray trace. The constants $\varkappa_1$ and $\varkappa_2$ may be calculated according to the method described in appendix F.

The present analysis can be applied to develop residual-error expressions associated with the Wachtell-DeFrate method also.

Applicability criterion. - The profiles $\frac{\varkappa_2}{\varkappa_1^2} b_2 L^2$ shown in figure 11 as a function of $b_2 L^2$ (cf. appendix F) are approximately straight lines with a slope of unity in the vicinity of the origin. Thus, $\frac{\varkappa_2}{\varkappa_1^2} \approx 1$, from which it follows that $|b_2| \ll 1$. However, for $\left|\left(\frac{\varkappa_2}{\varkappa_1^2}\right) b_2 L^2\right|$ sufficiently large, the profiles deviate drastically from a straight line thus indicating that $|b_2|$ increases considerably. In fact, when $d^2N/dy_D^2 < 0$, increasing values of $|b_2 L^2|$ eventually correspond to decreasing values of $\left|\left(\frac{\varkappa_2}{\varkappa_1^2}\right) b_2 L^2\right|$; this condition is absurd from practical considerations. The points at which the slopes of the profiles become zero $\left(d^2N/dy_D^2 < 0\right)$ may be considered, somewhat arbitrarily, as the extreme limits for which "true" values of b_2 are obtained. The defined limits correspond to fixed percentage deviations of the ratio $\varkappa_2/\varkappa_1^2$ from unity, namely

100% when $K = 1/3$

30% when $K = 1/2$

60% when $K = 1$

Let the preceding percentage deviations determine the practical limits of the profiles for $d^2N/dy_D^2 > 0$, also. Then because

$$\frac{\varkappa_2}{\varkappa_1^2} b_2 L^2 = \pm \frac{d^2N}{dy_D^2} \frac{\lambda L}{2}$$

the indicated limits correspond to

$$-4 < \pm \frac{d^2N}{dy_D^2} \frac{\lambda L}{2} < 7 \quad \text{when} \quad K = \frac{1}{3}$$

$$-0.8 < \pm \frac{d^2N}{dy_D^2} \frac{\lambda L}{2} < 0.8 \quad \text{when} \quad K = \frac{1}{2}$$

$$-0.4 < \pm \frac{d^2N}{dy_D^2} \frac{L}{2} < 0.3 \quad \text{when} \quad K = 1$$

3197

The inequalities listed in the section Applicability criterion result immediately from the preceding inequalities.

Test-section windows. - If the test section is bounded by windows, then mediums (-1) and (+1) correspond to the initial and final window, respectively, and the external atmosphere is contained in mediums (-2) and (+2). It has been demonstrated in reference 11 that, associated with an axial point-source, the additional optical-path differences contributed by the presence of windows are: in the final window,

$$\mu_g t \left[\sec \varphi\ (+1) - 1\right] \tag{E5}$$

and, in the atmosphere succeeding the test section,

$$\mu_a \left[KL - Z(t) + t\right] \left[1 - \sec \varphi\ (+2)\right] \tag{E6}$$

where μ_g is the refractive index of the window and t is the window thickness. The axial separation $Z(t)$ of the apparent- and real-object planes is given by

$$Z(t) = \left(1 - \frac{\mu_a}{\mu_g}\right)t \tag{E7}$$

for small angles φ, but is exact according to the initial assumption (1) in the section GENERALIZED EQUATIONS.

If off-axis source points are considered, then contributions (E5) and (E6) are replaced by

$$\mu_g t \left[\sec \varphi\ (+1) - \sec \varphi_r\ (+1)\right] \tag{E8}$$

and

$$\mu_a \left(KL + \frac{\mu_a}{\mu_g}\, t\right) \left[\sec \varphi_r\ (+2) - \sec \varphi\ (+2)\right] \tag{E9}$$

respectively, where $Z(t)$ has been replaced by the right side of expression (E7). The initial window introduces no additional contribution to the optical-path difference because associated ray traces are parallel within the window.

In reference 11 it has also been shown that terms (E5) and (E6), with the quantity KL omitted, cancel to a high order of approximation. With terms involving KL disregarded, the only possible additional terms of appreciable magnitude contributed by the window are, therefore,

3197 CM-5 back

$$\mu_g t \left[1 - \sec \varphi_r \, (+1)\right] \tag{E10}$$

and

$$\frac{\mu_a^2}{\mu_g} t \left[\sec \varphi_r \, (+2) - 1\right] \tag{E11}$$

These terms, which result from off-axis source points, also cancel if $\sec \varphi_r \, (+1)$ and $\sec \varphi_r \, (+2)$ are of the same order of magnitude as $\sec \varphi \, (+1)$ and $\sec \varphi \, (+2)$. The preceding cancellations result when φ_0 is zero, in which case the ray traces are given by

$$\sec \beta = \frac{\mu_\eta}{\mu_0}$$

If φ_0 is not zero, then the ray traces are given by

$$\sec \beta = \left[\left(\frac{\mu_\eta}{\mu_0}\right)^2 \sec^2 \varphi_0 - \tan^2 \gamma_0\right]^{1/2}$$

which is simply equation (C1a) rewritten. Thus, the preceding cancellations result when

$$\sec^2 \varphi_0 \approx 1$$

and

$$\tan^2 \gamma_0 \approx 0$$

or, in other words, when

$$\tan^2 \beta_0 = \left(\frac{q}{f}\right)^2 << 1$$

and

$$\tan^2 \gamma_0 = \left(\frac{p}{f}\right)^2 << 1$$

The only remaining term of appreciable magnitude is then

$$\mu_a KL \left[\sec \varphi_r \, (+2) - \sec \varphi \, (+2)\right]$$

which is actually the last term in equation (3).

3197

3197

APPENDIX F

THREE-TERM EVALUATION EQUATIONS ASSOCIATED WITH A ONE-DIMENSIONAL DISTRIBUTION $\rho(y)$

Assuming that $\mu_\eta = b_0 + b_1\eta + b_2\eta^2$, the evaluation equations associated with the three-term approximation are

(1) $$\rho^* = 1 + \frac{1}{k\rho_\infty}\left(N\frac{\lambda}{L} - \frac{1}{6}K_{2,3}b_1^2L^2 - \frac{1}{15}K_{2,5}b_1^2b_2L^4\right)$$

(2) $$y \equiv y_0 = y_D - D$$

(3) $$D = \pm\frac{1}{2}K_{1,2}b_1L^2 \pm \frac{1}{12}K_{1,4}b_1b_2L^2$$

(4) $$b_1 = \left|\frac{dN}{dy_D}\right|\frac{\varkappa_1}{\varkappa_2}\frac{\lambda}{L}$$

(5) $$\frac{\varkappa_2}{\varkappa_1^2}b_2L^2 = \pm\frac{d^2N}{dy_D^2}\frac{\lambda L}{2}$$

(6) $$\varkappa_1 = 1 + K_{1,2}b_2L^2 + \frac{1}{6}K_{1,4}(b_2L^2)^2$$

(7) $$\varkappa_2 = 1 + \frac{2}{3}K_{2,3}b_2L^2 + \frac{4}{15}K_{2,5}(b_2L^2)^2$$

The evaluation procedure is:

(1) Plot N as a function of y_D graphically from measured data.

(2) At each datum point measure slope dN/dy_D of the profile N_D.

(3) Plot dN/dy_D as a function of y_D.

(4) At each datum point measure slope d^2N/dy_D^2 of the profile dN/dy_D.

(5) For each datum point compute $(\varkappa_2/\varkappa_1^2)b_2L^2$.

(6) Select appropriate plot of b_2L^2 as a function of $(\varkappa_2/\varkappa_1^2)b_2L^2$ from figure 11(a) or 11(b), depending upon the algebraic sign of d^2N/dy_D^2, and determine the value of b_2L^2 which corresponds to the appropriate value of K and to the computed value of $(\varkappa_2/\varkappa_1^2)b_2L^2$. (Plots of $(\varkappa_2/\varkappa_1^2)b_2L^2$ as a function of b_2L^2 are given in figures 11(a) and (b) for K = 1/3, 1/2, and 1 and for $d^2N/dy_D^2 > 0$ and $d^2N/dy_D^2 < 0$.)

(7) For each datum point compute $b_2 = (b_2L^2)/L^2$.

(8) For each datum point compute $\varkappa_1$ and $\varkappa_2$.

(9) For each datum point compute b_1, then ρ^*, D, and y_0.

The density ratio ρ^* as a function of y represents the desired profile.

The measured quantity N and the computed quantities dN/dy_D, d^2N/dy_D^2 are associated with the measured profile N_D and values y_D. All other quantities which are functions of y are associated with distortionless values $y_0 = y$.

The profiles $(\varkappa_2/\varkappa_1^2)b_2L^2$ as a function of b_2L^2 were obtained by choosing values of b_2L^2, computing $\varkappa_1$, $\varkappa_2$, and then $(\varkappa_2/\varkappa_1^2)b_2L^2$ for a given value of K. Thus, profiles can be readily determined for other values of K.

3197

APPENDIX G

EQUATIONS FOR CALCULATING PROFILE N_D ASSOCIATED WITH A HYPOTHETICAL EXPONENTIAL-DENSITY PROFILE

In order to calculate the profile N_D associated with an assumed hypothetical profile $\rho(y)$, the assumed profile $\rho(y)$ must be selected such that

$$L = \int_0^H \frac{d\eta}{\sqrt{\left(\frac{\mu_\eta}{\mu_0}\right)^2 - 1}} = \int_{y_0}^{y_0+H} \frac{dy}{\sqrt{\left[\frac{\mu(y)}{\mu(y_0)}\right]^2 - 1}} \quad \left[\mu(y) \geqq \mu(y_0)\right] \qquad (G1)$$

and

$$\int_0^L \Delta\mu_\eta d\zeta$$

which are involved in computing N_D, are readily integrable in exact, or nearly exact, form. Among possible assumed distributions $\rho(y)$ an exponential function, which corresponds to the refractive-index distribution

$$\mu = \mu_\infty - (\mu_\infty - \mu_w)e^{-y/a}$$

where $\mu = \mu_w$ at $y = 0$, and a is an arbitrary constant, permits the required integrations and corresponds vaguely to a possible boundary-layer profile.

With an exponential density distribution and an axial point source assumed, the ray-trace displacements H at $\zeta = L$ are given by the solution of equation (G1), namely

$$H = a \ln\left[\frac{1}{2}(1 + \cosh t)\right] \qquad (G2)$$

where

$$t = \frac{L}{a}\sqrt{2(\mu_\infty - \mu_w)}\, e^{-y_0/2a}$$

The ray traces satisfy

$$y = y_0 \quad \text{at} \quad \zeta = 0$$

$$y = y_L \quad \text{at} \quad \zeta = L$$

where

$$y_L = y_0 + H$$

At $y = y_0$,

$$\mu(y_0) = \mu_\infty - (\mu_\infty - \mu_w)e^{-y_0/a} \tag{G3a}$$

At $y = y_L$,

$$\mu(y_L) = \mu_\infty - (\mu_\infty - \mu_w)e^{-y_L/a} \tag{G3b}$$

The fringe shifts and distortions are given by equations (C12) and (C11), respectively, which become in the present instance

$$N = [\mu_\infty - (1 - K)\,\mu(y_0) - K\,\mu(y_L)]\frac{L}{\lambda} - 2\,\frac{a^2 t}{\lambda L}\tanh\left(\frac{t}{2}\right) \tag{G4}$$

$$D = H - \sqrt{2[\mu(y_L) - \mu(y_0)]\,KL} \tag{G5}$$

In order to recompute $\rho^*(y)$, values of the derivatives d^nN/dy_D^n must be determined. Theoretical values of d^nN/dy_D^n can be computed. Derivatives d^nN/dy^n are obtained by differentiating equation (G4), with $\mu(y_0)$ and $\mu(y_L)$ replaced by the right side of equations (G3a) and (G3b), respectively. The required first two derivatives are given by

$$\left(\frac{dN}{dy}\right)_{y_0} = -\left[(1 - K)\left(\frac{d\mu}{dy}\right)_{y_0} + K\left(\frac{d\mu}{dy}\right)_{y_L}\left(1 + \frac{dH}{dy}\right)\right]\frac{L}{\lambda} + \frac{4a^2}{\lambda L}\,\frac{d^2H}{dy^2} \tag{G6a}$$

$$\left(\frac{d^2N}{dy^2}\right)_{y_0} = -\left\{(1-K)\left(\frac{d^2\mu}{dy^2}\right)_{y_0} + K\left[\left(\frac{d\mu}{dy}\right)_{y_L}\frac{d^2H}{dy^2} + \left(\frac{d^2\mu}{dy^2}\right)_{y_L}\left(1+\frac{dH}{dy}\right)^2\right]\right\}\frac{L}{\lambda} + \frac{4a^2}{\lambda L}\,\frac{d^3H}{dy^3} \tag{G6b}$$

3197

where

$$\left(\frac{d\mu}{dy}\right)_{y_0} = \frac{\mu_\infty - \mu(y_0)}{a} \tag{G7a}$$

$$\left(\frac{d^2\mu}{dy^2}\right)_{y_0} = -\frac{1}{a}\left(\frac{d\mu}{dy}\right)_{y_0} \tag{G7b}$$

and

$$\left(\frac{d\mu}{dy}\right)_{y_L} = \frac{\mu_\infty - \mu(y_L)}{a} \tag{G8a}$$

$$\left(\frac{d^2\mu}{dy^2}\right)_{y_L} = -\frac{1}{a}\left(\frac{d\mu}{dy}\right)_{y_L} \tag{G8b}$$

Derivatives d^nH/dy^n follow from equation (G2). Thus,

$$\frac{dH}{dy} = a\,\frac{\sinh t\,\dfrac{dt}{dy}}{1 + \cosh t} \tag{G9a}$$

$$\frac{d^2H}{dy^2} = a\,\frac{\left(\dfrac{dt}{dy}\right)^2 + \sinh t\,\dfrac{d^2t}{dy^2}}{1 + \cosh t} \tag{G9b}$$

$$\frac{d^3H}{dy^3} = -\frac{1}{2a}\left[\frac{t^2}{4a}\left(1 + \frac{dH}{dy}\right)\operatorname{sech}^2\frac{t}{2} + \frac{d^2H}{dy^2}\right] \tag{G9c}$$

where

$$\frac{dt}{dy} = \frac{-t}{2a} \tag{G10a}$$

$$\frac{d^2t}{dy^2} = \frac{t}{4a^2} \tag{G10b}$$

3197 CM-6

Derivatives d^nN/dy_D^n are functions of derivatives d^nN/dy^n given by equation (D3) and the recurrence formula (D4). The required first two derivatives of D are obtained by differentiating equation (G5) following the previously mentioned substitutions for $\mu(y_O)$ and $\mu(y_L)$. Then,

$$\frac{dD}{dy} = \frac{dH}{dy} + 2aK\frac{d^2H}{dy^2} \tag{G11a}$$

$$\frac{d^2D}{dy^2} = \frac{d^2H}{dy^2} + 2aK\frac{d^3H}{dy^3} \tag{G11b}$$

3197

The profile N_D is determined by computing equations (G1) to (G5), and the derivatives d^nN/dy_D^n $(n = 1,2)$ are calculated from equations (G6) to (G11).

The selected values of the constants were

$\mu_\infty = 1.0000792$ ($\rho_\infty = 6.77\times10^{-4}$ slug/ft^3)

$\mu_w = 1.0000475$ ($\rho_w = 4.06\times10^{-4}$ slug/ft^3)

$a = 0.0058$ in.

$\lambda = 2.15\times10^{-5}$ in. (mercury green line)

$\varkappa = 0.117$ ft^3/slug

which, except for a, are identical to the values involved in the example of reference 11.

3197

CM-6, back,

APPENDIX H

EXPERIMENTAL VERIFICATION OF REFRACTION EFFECT

The conduction of heat by air between two horizontal surfaces provides a readily produced and reasonably predictable density distribution which may be utilized for verifying the refraction effect and two-term evaluation equations. Consider two identical rectangular-shaped blocks placed one above the other and separated by a small distance, with facing surfaces A and B corresponding to the bottom surface of the top block and the top surface of the bottom block, respectively. Suppose that both blocks contain a reference hole which extends throughout the horizontal length of the block and is oriented parallel to the optical axis of the interferometer.

When the upper block is heated, a constant temperature gradient is produced in the airspace between the blocks, whereas the temperatures within the reference holes are constants. If the blocks are good heat conductors, then the temperature T_1 within the reference hole through the upper block and the temperature T_A at surface A are equal. However, $(d\rho/dy)_1 = 0$ whereas $(d\rho/dy)_A$ = constant $\neq 0$, so that light which traverses the space between the blocks is refracted whereas light which traverses the reference hole is not. Thus, the optical-path difference between light passing adjacent to A and light traversing the reference hole should theoretically be given by

$$N_A = \frac{1}{6} K_{2,3} \left(\frac{dN}{dy_D}\right)_A^2 \lambda^2 L \tag{H1}$$

and the distortion should be given by

$$D_A = \frac{1}{2} K_{1,2} \left(\frac{dN}{dy_D}\right)_A \lambda L \tag{H2}$$

These equations contain only contributions attributable to refraction.

In order to properly associate the refraction and reference fringes, the algebraic sign of the fringe shift corresponding to the reference region in the lower block must be determined. Because $T_2 < T_1$, where T_2 is the temperature of the lower block, $\mu_2 > \mu_1$, so that $N_2 > 0$. Therefore, it follows from equation (H1) that:

(1) If $K < 2/3$, then $N_A > 0$ and the fringes between the blocks are displaced toward the zero-order fringe in the lower reference region (fig. 12(a)).

(2) If $K = 2/3$, then $N_A = 0$, that is, no fringe shift occurs (fig. 12(b)).

(3) If $K > 2/3$, then $N_A < 0$ and the fringes are displaced away from the zero-order fringe in the lower reference region (fig. 12(c)). A corresponding interferogram utilizing unfiltered light will permit the zero-order fringe to be distinguished.

3197

The model shown in figure 13 was constructed in order to simulate the aforementioned conditions. The model consists of two Duraluminum blocks 10-inches long which are separated by two 0.14-inch thick, 10-inch long insulating strips of glass. The top surface of the upper block is radiant-heated by a Nichrome-wire heater consisting of Nichrome resistance wire wound with varying pitch around a thin sheet of mica. The heating element and most of the upper block are insulated from the external atmosphere by a Transite lid in order that the heat-flow rate from the upper block to the lower block will be a maximum for any given heating current. A reference hole was machined the length of each block, and a reference pin was projected into each reference hole for focussing purposes and as a measuring reference.

Figures 14(a) and (b) depict typical interferograms of the heated air for $K = 1/2$ and 1, respectively; these interferograms were obtained by utilizing unfiltered light from a magnesium spark in conjunction with a horizontal slit. It is apparent that the temperature gradient between the blocks is nearly constant. Curvature of the fringes near the upper surface of the lower block is caused by reflection.

In figures 15(a) and (b), experimentally determined values of optical-path differences and distortion, respectively, are compared with theoretical values indicated by equations (H1) and (H2). The quantities $N_A\lambda$ and D_A are plotted with respect to the generalized coordinate $(dN/dy_D)_A\lambda$ which yields a single curve for all wave lengths λ. Actually, the experimental data include measurements at two wave lengths, namely 4481 Å (magnesium spark) and 5461 Å (mercury arc). Agreement of the experimentally determined points with the predicted curves is regarded as good considering the errors involved in the experiment and the fact that the difference in values amounts to the error of measuring a small error.

The most important experimental errors probably were end effects, thermal expansion of the apparatus, nonuniform heating of the apparatus, inclination of reference fringes, and poor definition of the apparent location of surface A.

In attempting to minimize end effects, the model was initially bounded by 0.8-inch-thick glass windows separated from the model ends by thin cork spacers. The windows were slid into position immediately preceding each photographic exposure. The experimental data were then in poor agreement with theory. Apparently, insertion of the windows prior to the photographic exposure, even for very short periods of time, allowed appreciable nonuniform heating of the glass. Air disturbances were not evident. It would appear that extreme caution should be exercised in interpreting interferograms of heated models when the model contacts bounding glass windows. In order to eliminate the window effects, the windows were removed, and the ends were left unbounded. A new set of measurements rendered the results presented in figures 15(a) and (b). The interference pattern obtained across the end of the model with the open-end arrangement was examined visually while the model was heated. The endwise boundary layer was found to be of nearly constant thickness (about 1/4 inch) in the region of interest, and the temperature gradient was essentially parallel to the model length at all pertinent temperatures. Thus, the end effects were regarded as inappreciable when the windows were removed.

3197

Thermal expansion of the model was considered in the vertical direction, but expansion in the lengthwise direction was neglected.

Temperatures were measured throughout the model by means of thermocouples located at the points indicated in figure 13(b). A typical temperature distribution is also indicated in the figure, where the temperature difference at each point is noted with respect to the uppermost thermocouple location in the midspan plane. Inclination of reference fringes with respect to surface A, caused by initial misorientation of the fringes and the small vertical temperature gradient within the upper block, was considered in the measurements.

The existence of refracted ray traces in the vicinity of surface A tended to diminish the definition of the apparent surface location. The difficulty of locating surface A, especially when $K = 1/2$, may account for the apparent systematic disagreement between theory and experiment when $K = 1/2$.

REFERENCES

1. Winckler, John R.: The Mach Interferometer Applied to Studying an Axially-Symmetric Supersonic Air Jet. Rev. Sci. Inst., vol. 19, no. 5, May 1948, pp. 307-322.

2. Eckert, E. R. G., and Soehngen, E. E.: Studies on Heat Transfer in Laminar Free Convection with the Zehnder-Mach Interferometer. Tech. Rep. 5747, A.T.I. No. 44580, Air Materiel Command, Wright-Patterson Air Force Base, Dayton (Ohio), Dec. 27, 1948.

3. Ladenburg, R., and Bershader, D.: On Laminar and Turbulent Boundary Layer in Supersonic Flow. Rev. Mod. Phys., vol. 21, no. 3, July 1949, pp. 510-515.

4. Gooderum, Paul B., Wood, George P., and Brevoort, Maurice J.: Investigation with an Interferometer of the Turbulent Mixing of a Free Supersonic Jet. NACA Rep. 963, 1950. (Supersedes NACA TN 1857.)

5. Kovasznay, Leslie S. G., and Clarken, Patricia C.: Experimental Investigation of Optical Methods for Measuring Turbulence. Tech. Rep. No. 42, Proj. Squid, Johns Hopkins Univ., Jan. 1, 1952. (Office Naval Res., Dept. Navy, Res. and Dev. Command, Dept. Air Force Contract N6ori-105, Task Order III, NR-098-038.)

6. Lin. C. S., Mouton, R. W., and Putnam, G. L.: Mass Transfer Between Solid Wall and Fluid Streams. Ind. and Eng. Chem., vol. 45, no. 3, Mar. 1953, pp. 636-640.

7. Wachtell, G. P.: Refraction Effect in Interferometry of Boundary Layer of Supersonic Flow Along Flat Plate. Appendix to: Prog. Rep. No. 19, The Study of Supersonic Flow by Interferometry and Other Optical Methods by R. Ladenburg. Palmer Phys. Lab., Princeton Univ., Dec. 19, 1949. (Contract N7 ONR 399, Task Order 1.)

8. DeFrate, Louis A.: Application of the Interferometer to the Study of Boundary Layers. Sc. D. Thesis, M.I.T. 1950.

9. Wachtell, George Peter: Refraction Error in Interferometry of Boundary Layer in Supersonic Flow Along a Flat Plate. Ph. D. Thesis, Princeton Univ., 1951.

10. Wachtell, G. P.: The Refraction Problem. Pt. VIII in Optical Studies of Boundary Layer Phenomena on a Flat Plate at Mach Number 2.35 by R. Ladenburg and D. Bershader. Final Tech. Rep. NR061-020, Palmer Phys. Lab., Princeton Univ., Dec. 15, 1952, pp. 81-124. (Contract N6ori-105, Task II.)

11. Howes, Walton L., and Buchele, Donald R.: A Theory and Method for Applying Interferometry to the Measurement of Certain Two-Dimensional Gaseous Density Fields. NACA TN 2693, 1952.

12. Jenkins, Francis A., and White, Harvey E.: Fundamentals of Physical Optics. First ed., McGraw-Hill Book Co., Inc., 1937, p. 79.

13. Schardin, H.: Theory and Applications of the Mach-Zehnder Interference-Refractometer. Rep. T-3, Defense Res. Lab., Univ. of Texas, 1946.

3197

14. Ladenburg, R., Van Voorhis, C. C., and Winckler, J.: Interferometric Study of Supersonic Phenomena. Pt. I: A Supersonic Air Jet at 60 lb/in^2 Tank Pressure. NAVORD Rep. 69-46, Bur. Ord., Navy Dept., Apr. 17, 1946. (See also Phys. Rev., vol. 76, no. 5, Sept. 1949, pp. 662-677.)

15. Bennett, F. D., Carter, W. C., and Bergdolt, V. E.: Interferometric Analysis of Airflow about Projectiles in Free Flight. Jour. Appl. Phys., vol. 23, no. 4, Apr. 1952, pp. 453-469.

16. Blue, Robert E.: Interferometer Corrections and Measurements of Laminar Boundary Layers in Supersonic Stream. NACA TN 2110, 1950.

17. Bershader, Daniel: An Interferometric Study of Supersonic Channel Flow. Rev. Sci. Inst., vol. 20, no. 4, Apr. 1949, pp. 260-275.

18. Luneberg, R. K.: Mathematical Theory of Optics. Advanced Instruction and Research in Mechanics, Brown Univ., Providence (R. I.), 1944.

3197

3197

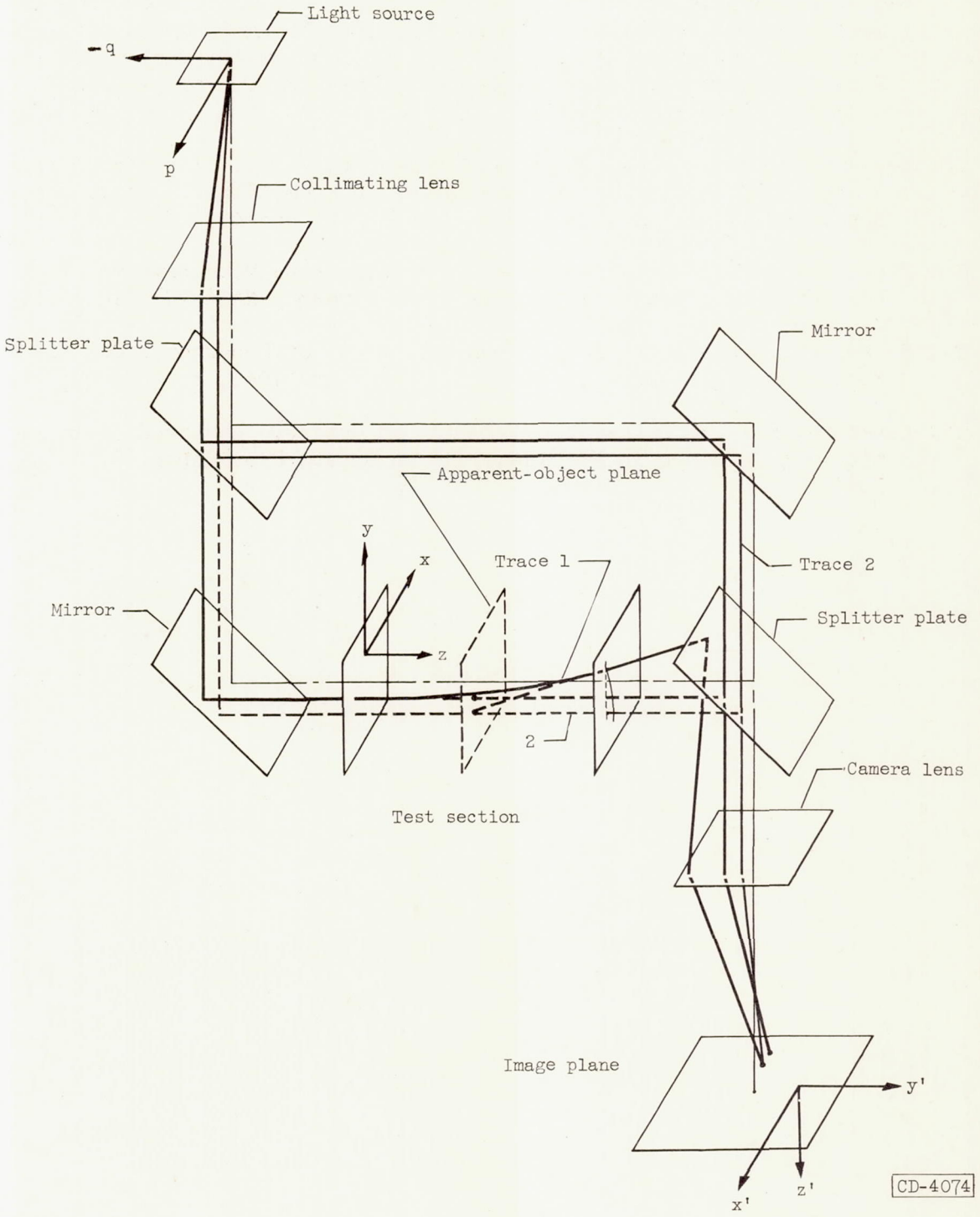


Figure 1. - Zehnder-Mach interferometer and characteristic ray traces.

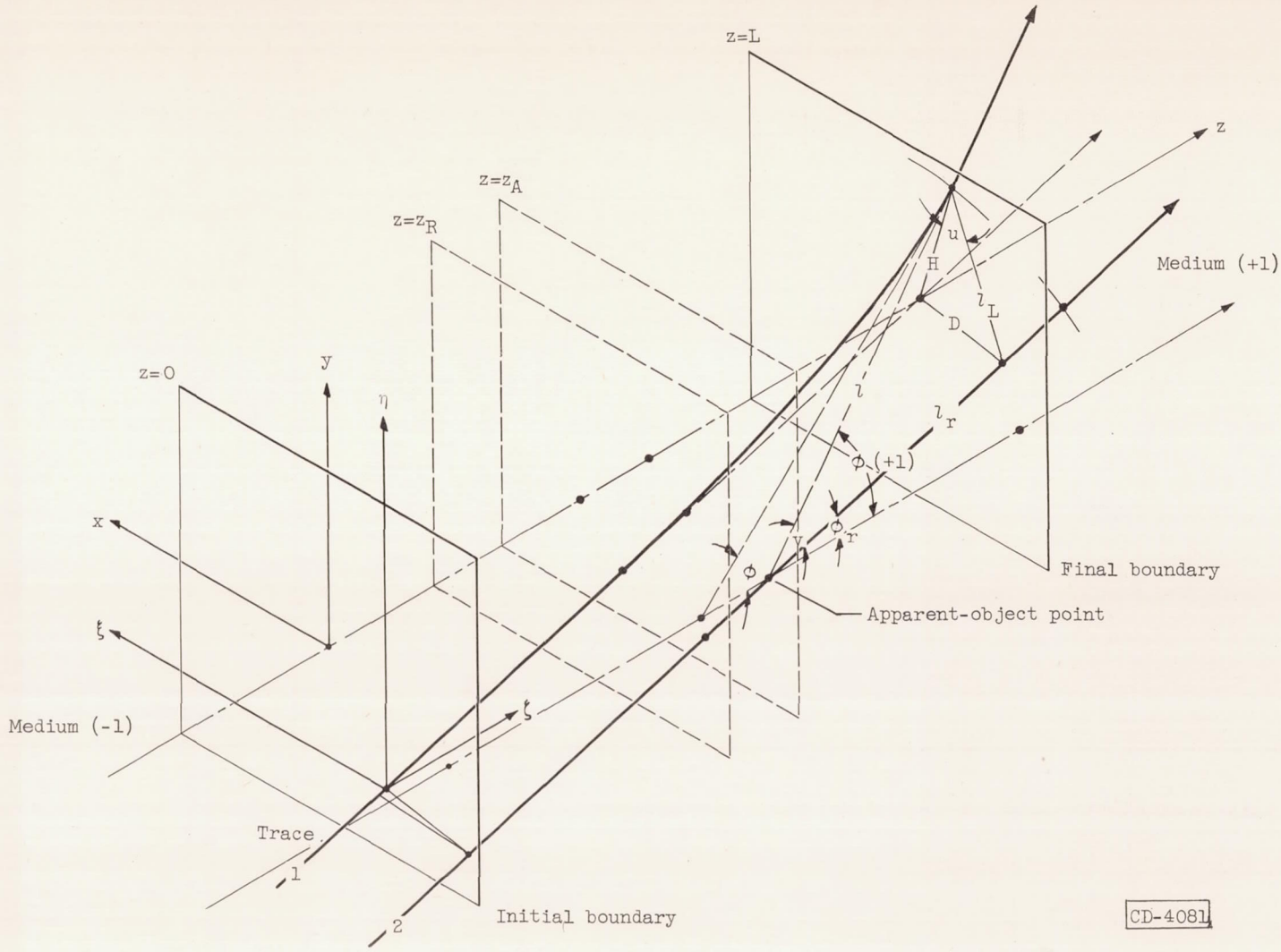


Figure 2. - Light-path detail within test section.

3197

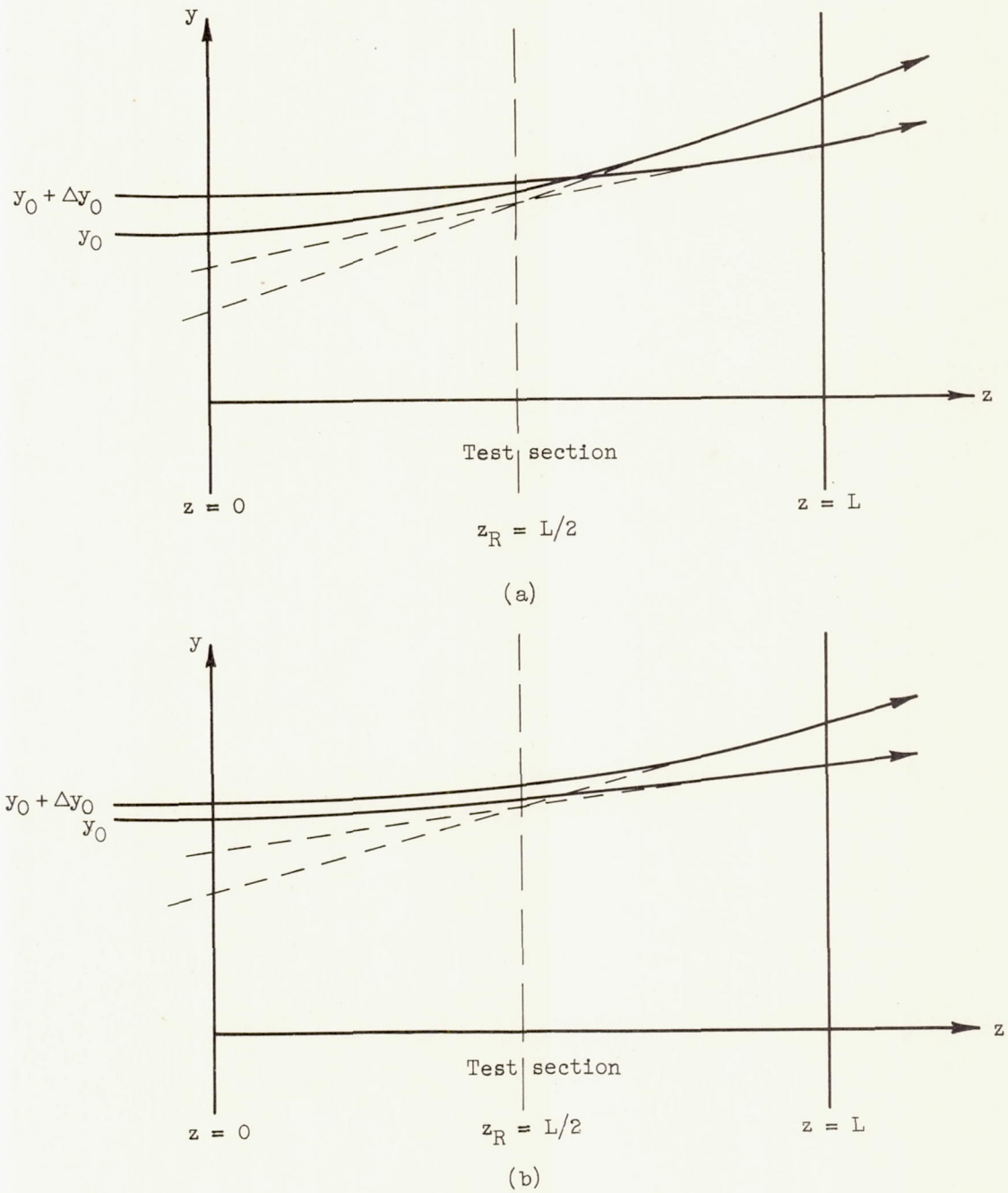


Figure 3. - Examples of apparent-ray-trace crossing.

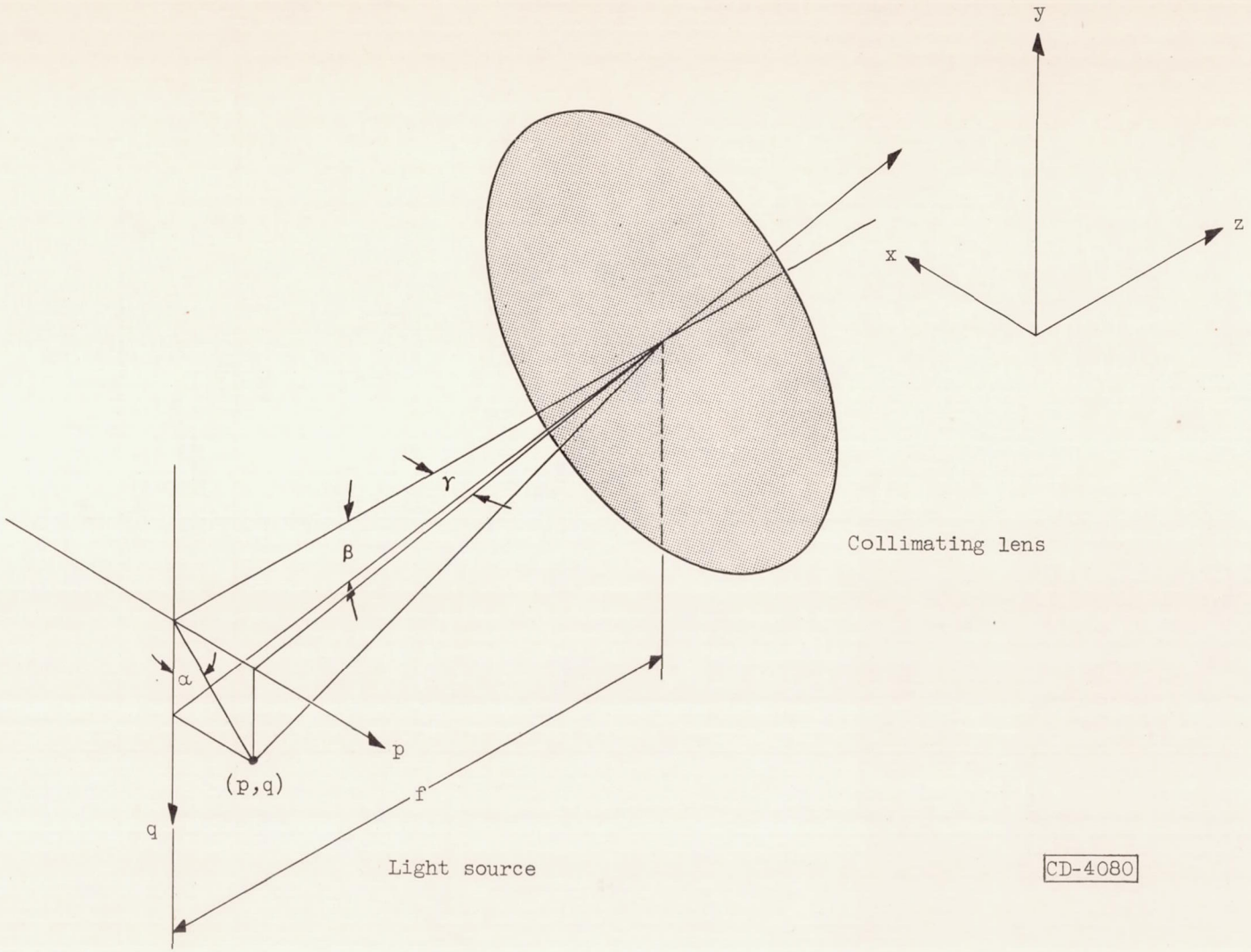
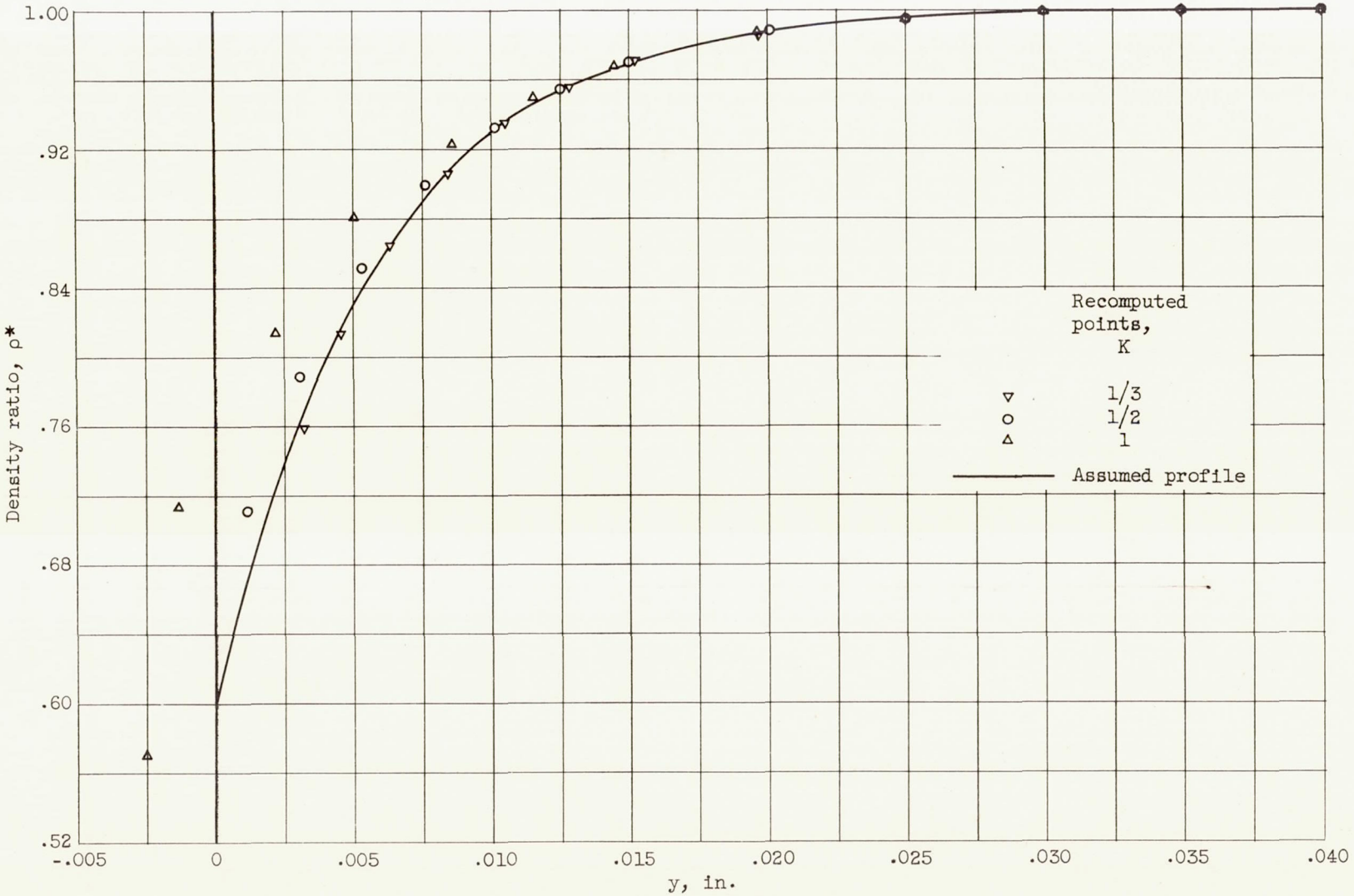
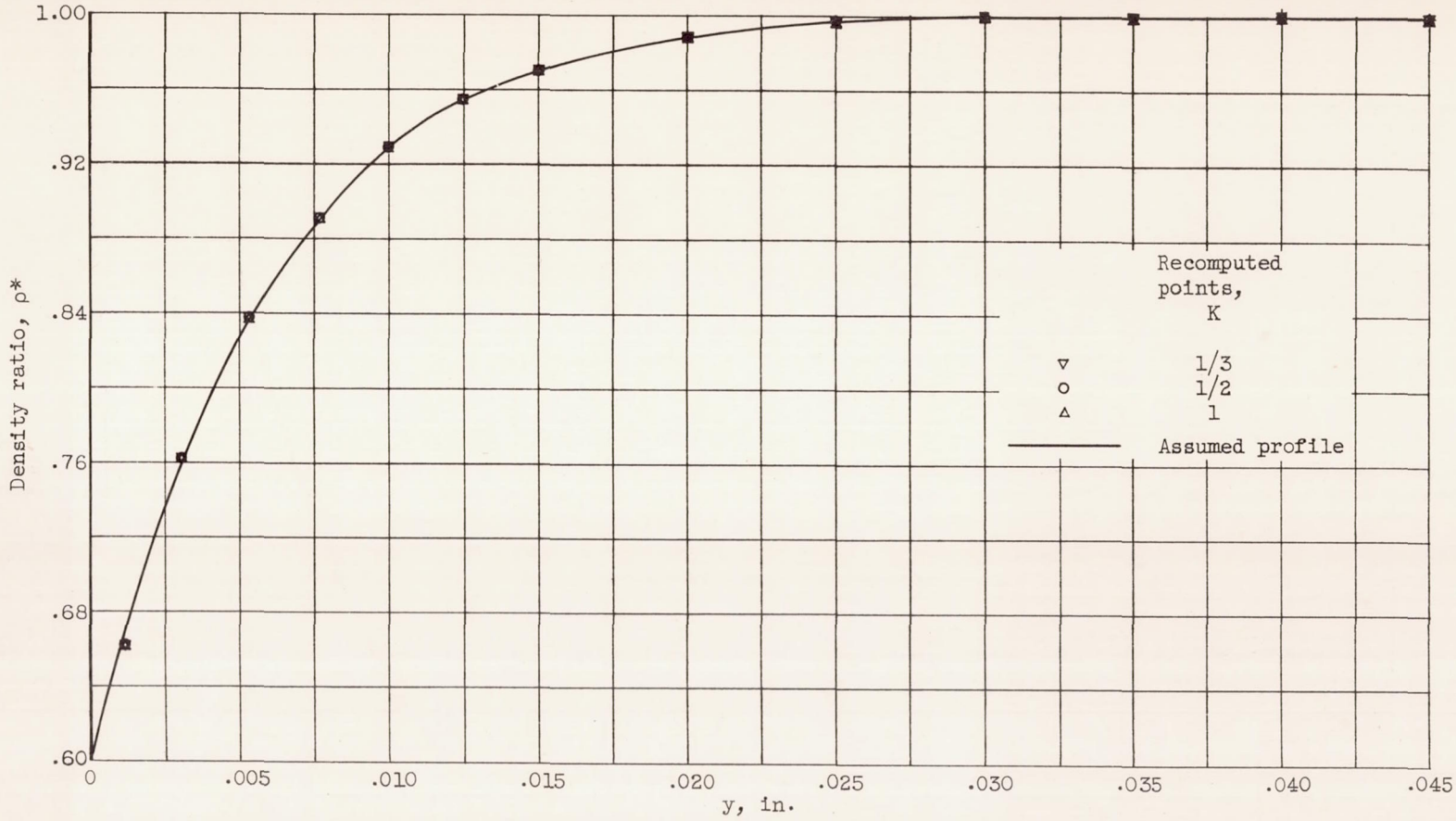


Figure 4. - Light-path detail preceding collimating lens.



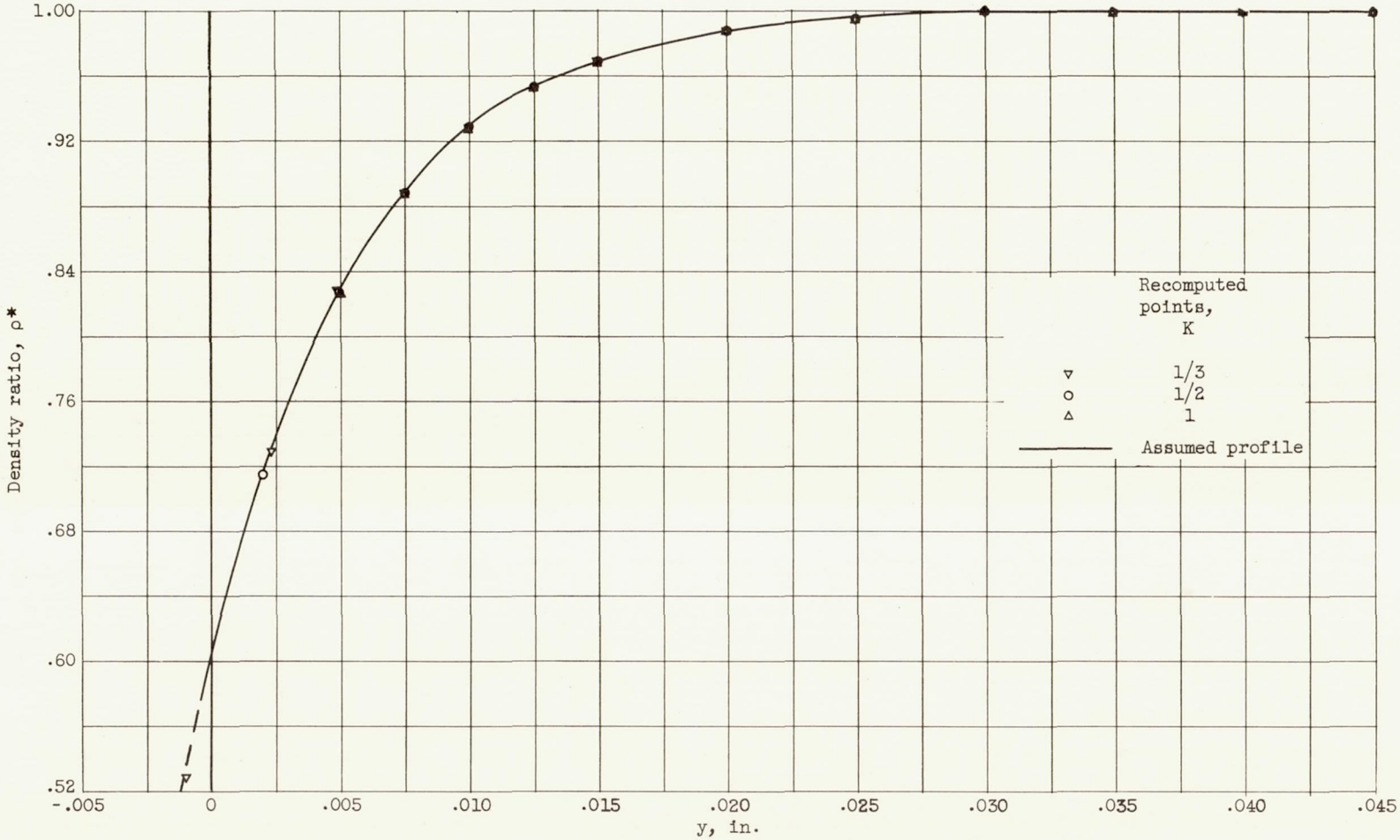
(a) One-term approximation.

Figure 5. - Re-evaluation of exponential density profile where L = 1.8 inches.



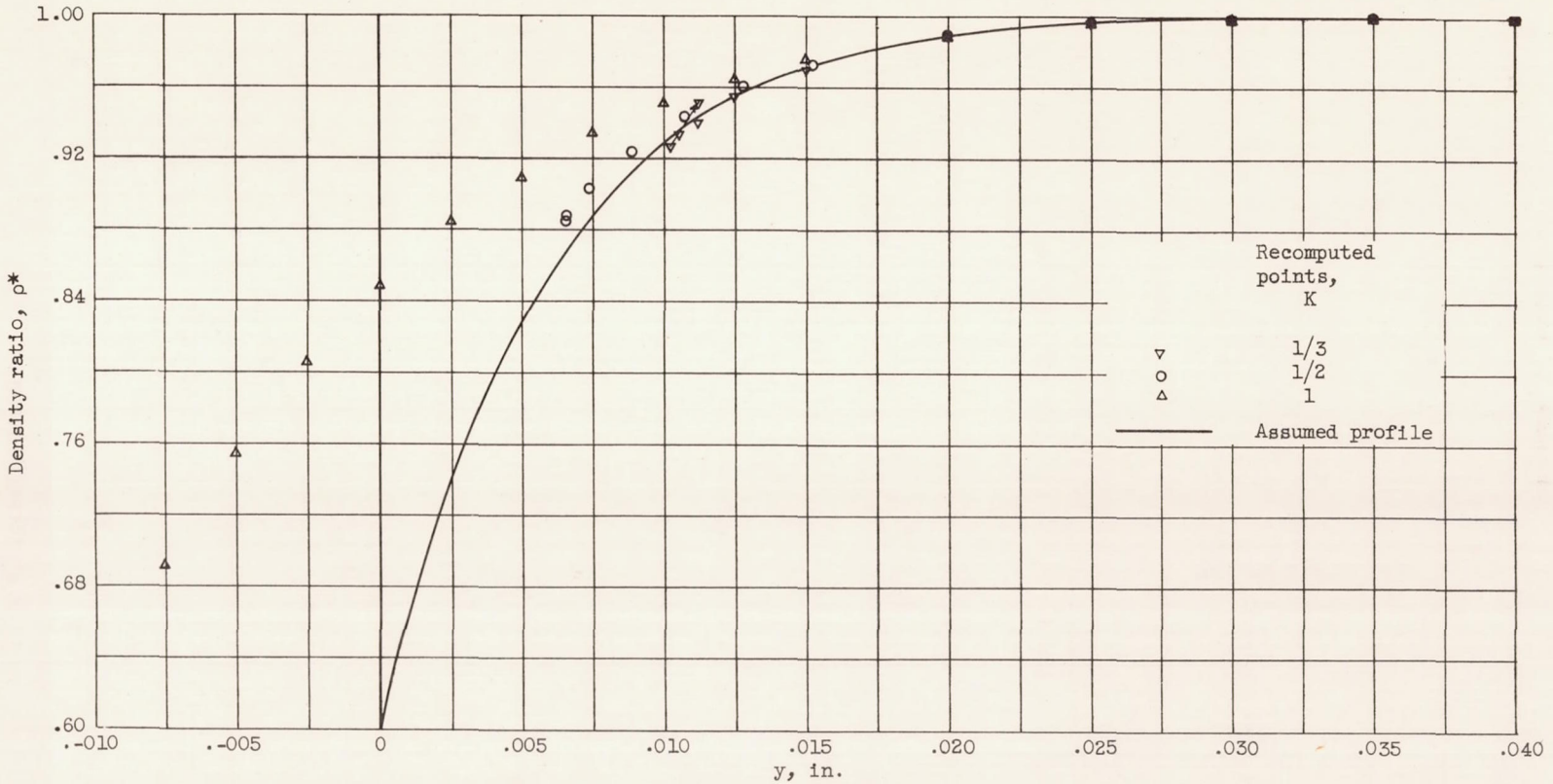
(b) Two-term approximation.

Figure 5. - Continued. Re-evaluation of exponential density profile where L = 1.8 inches.



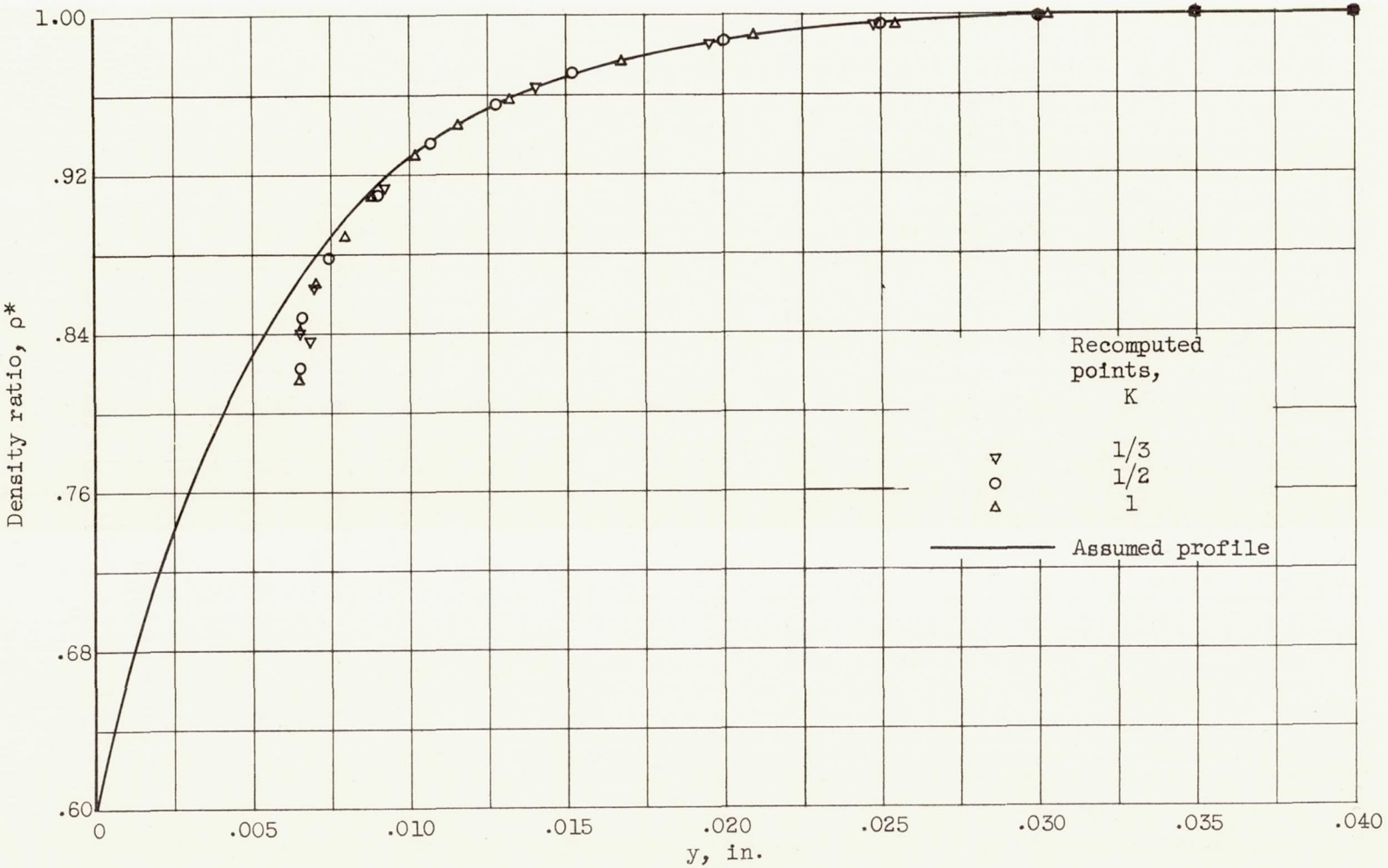
(c) Three-term approximation.

Figure 5. - Concluded. Re-evaluation of exponential density profile where L = 1.8 inches.



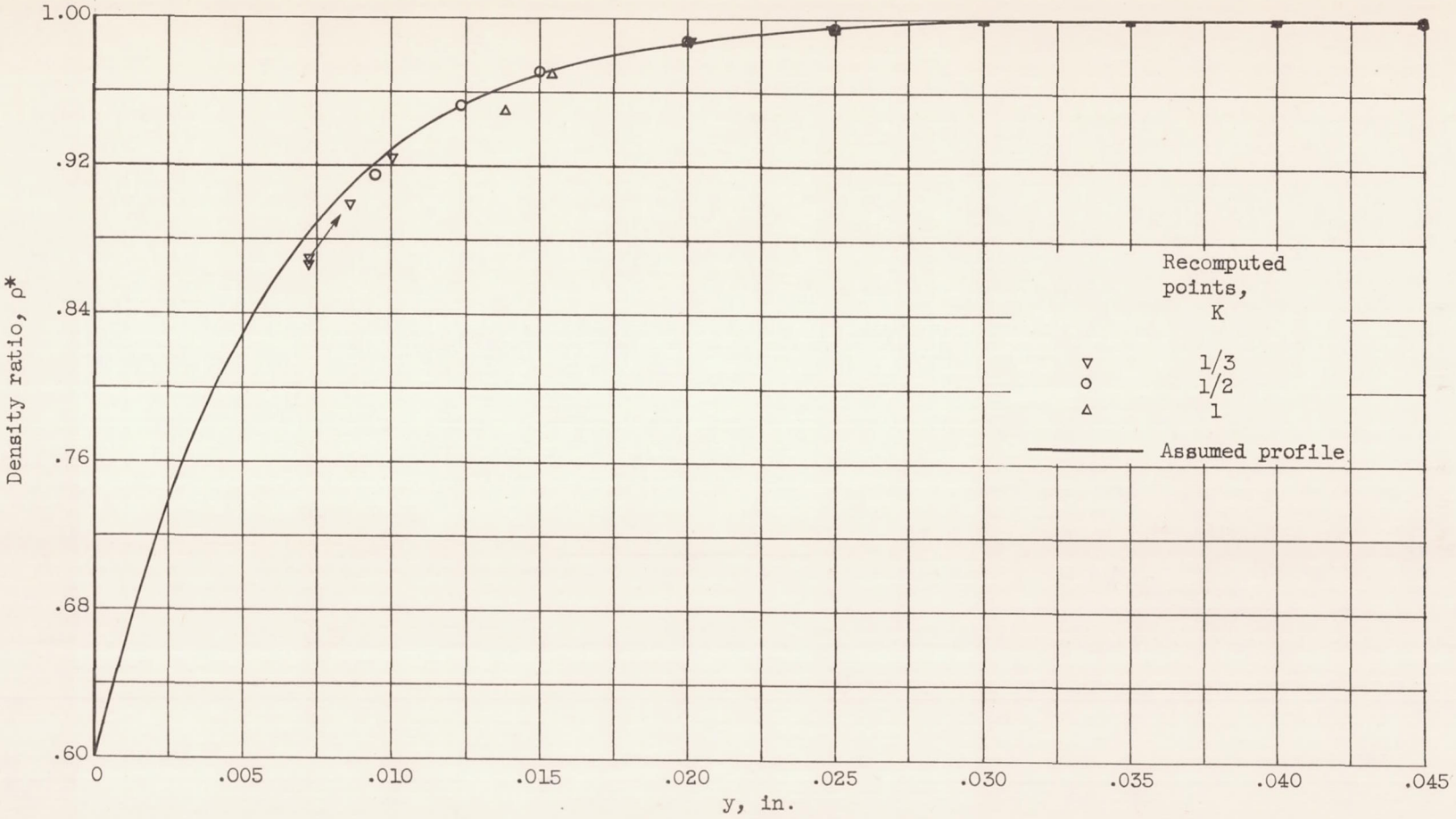
(a) One-term approximation.

Figure 6. - Re-evaluation of exponential density profile where L = 3.6 inches.



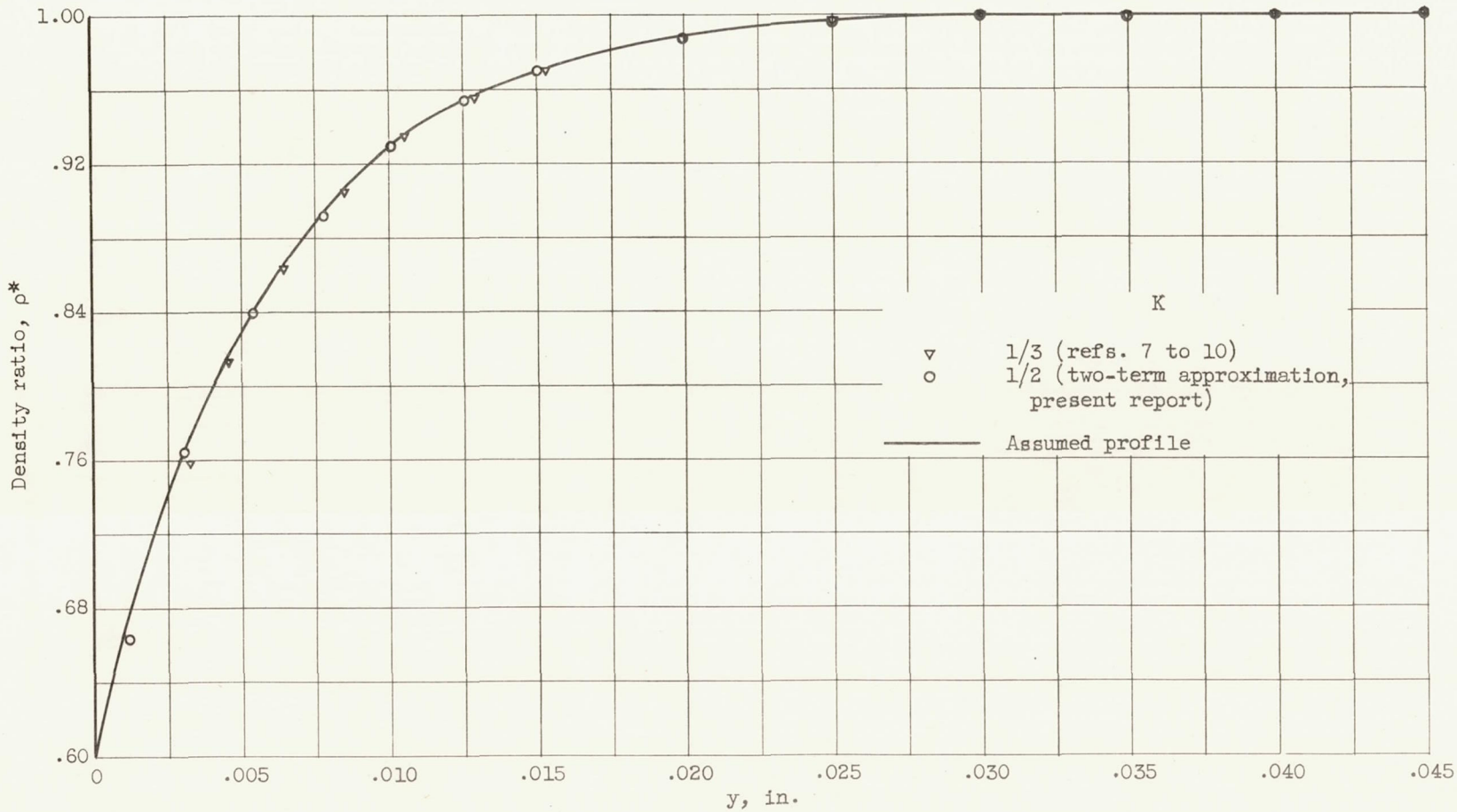
(b) Two-term approximation.

Figure 6. - Continued. Re-evaluation of exponential density profile where L = 3.6 inches.



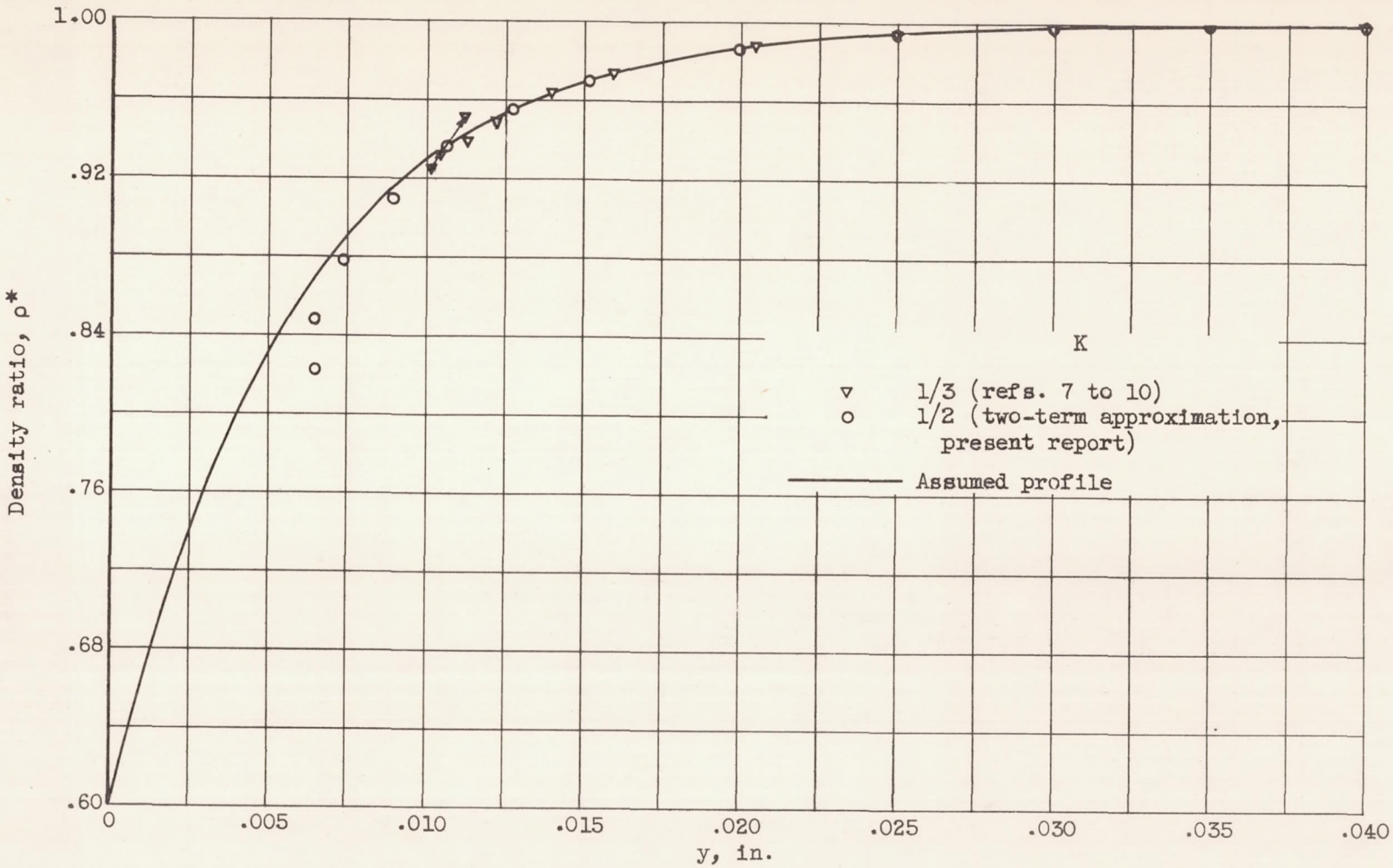
(c) Three-term approximation.

Figure 6. - Concluded. Re-evaluation of exponential density profile where L = 3.6 inches.



(a) L = 1.8 inches.

Figure 7. - Comparison of re-evaluated density profiles.



(b) L = 3.6 inches.

Figure 7. - Concluded. Comparison of re-evaluated density profiles.

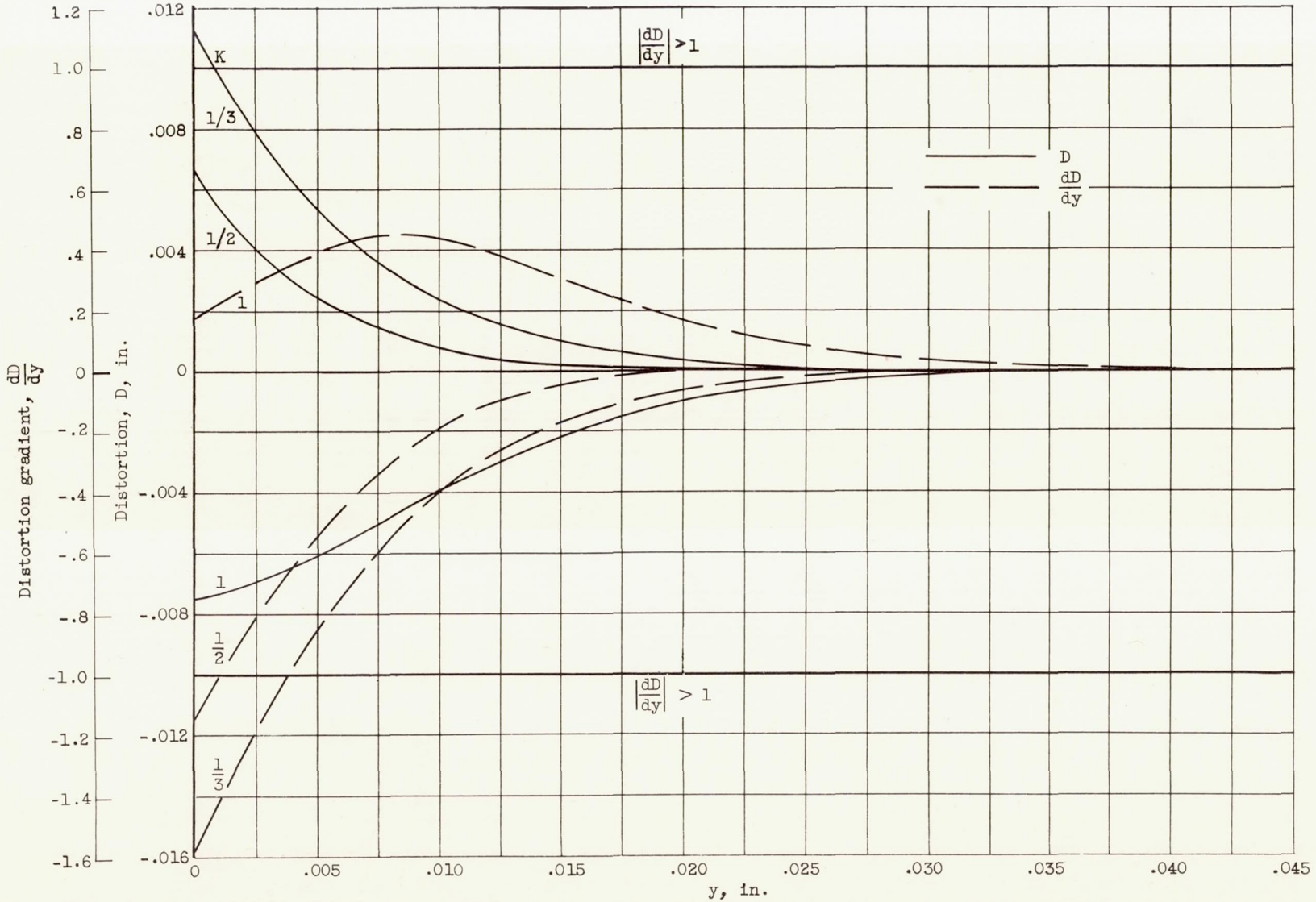
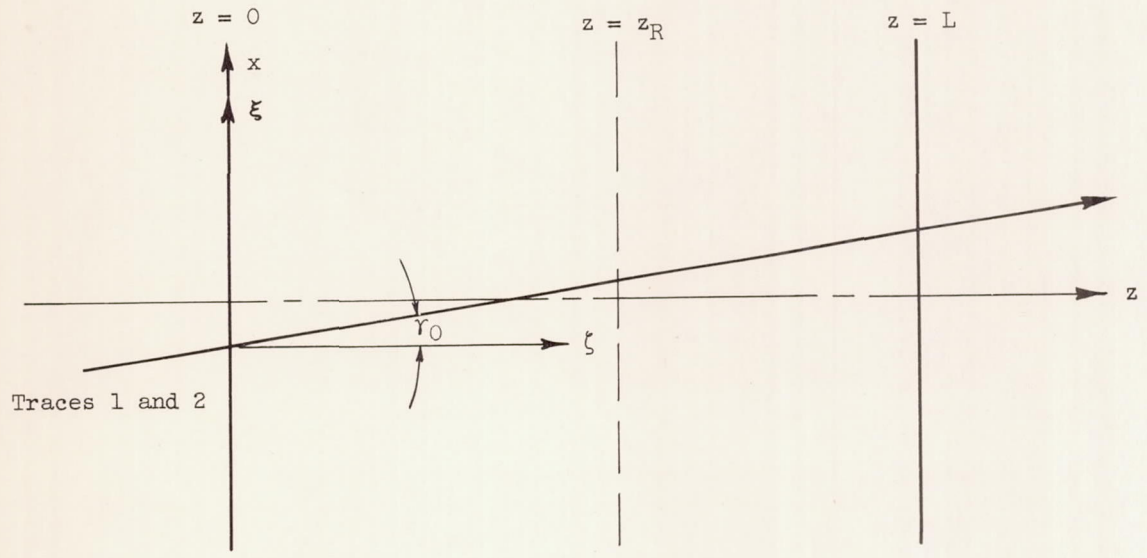
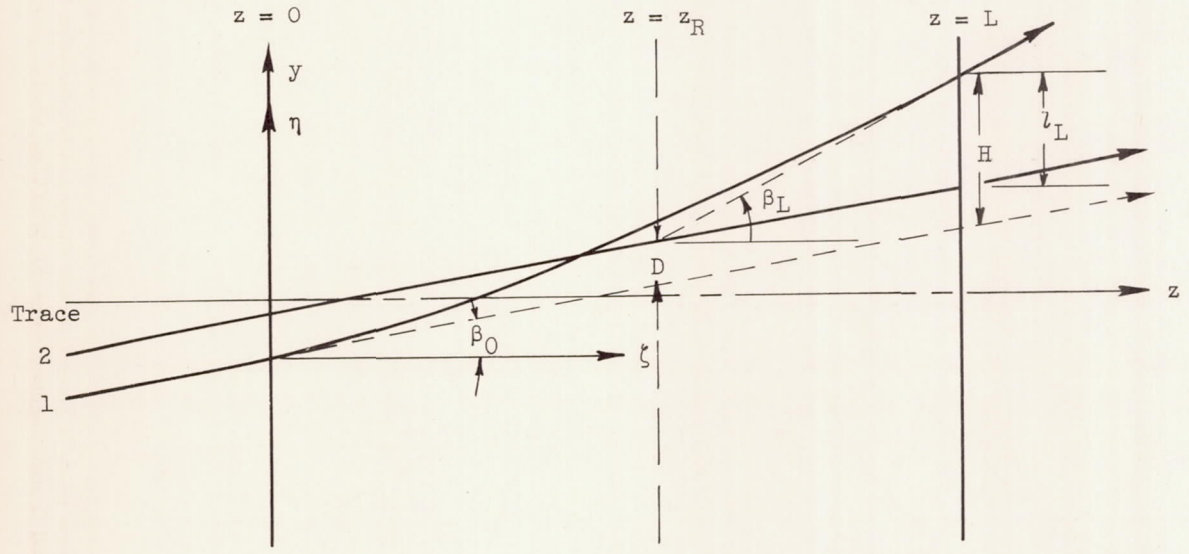


Figure 8. - Distortion and distortion gradient associated with object planes corresponding to K = 1/3, 1/2, and 1 and assumed density profile, where L = 3.6 inches.

3197



(a) Projection in xz-plane.



(b) Projection in yz-plane.

Figure 9. - Ray-trace projections in presence of a unidirectional distribution $\mu = \mu(y)$.

3197

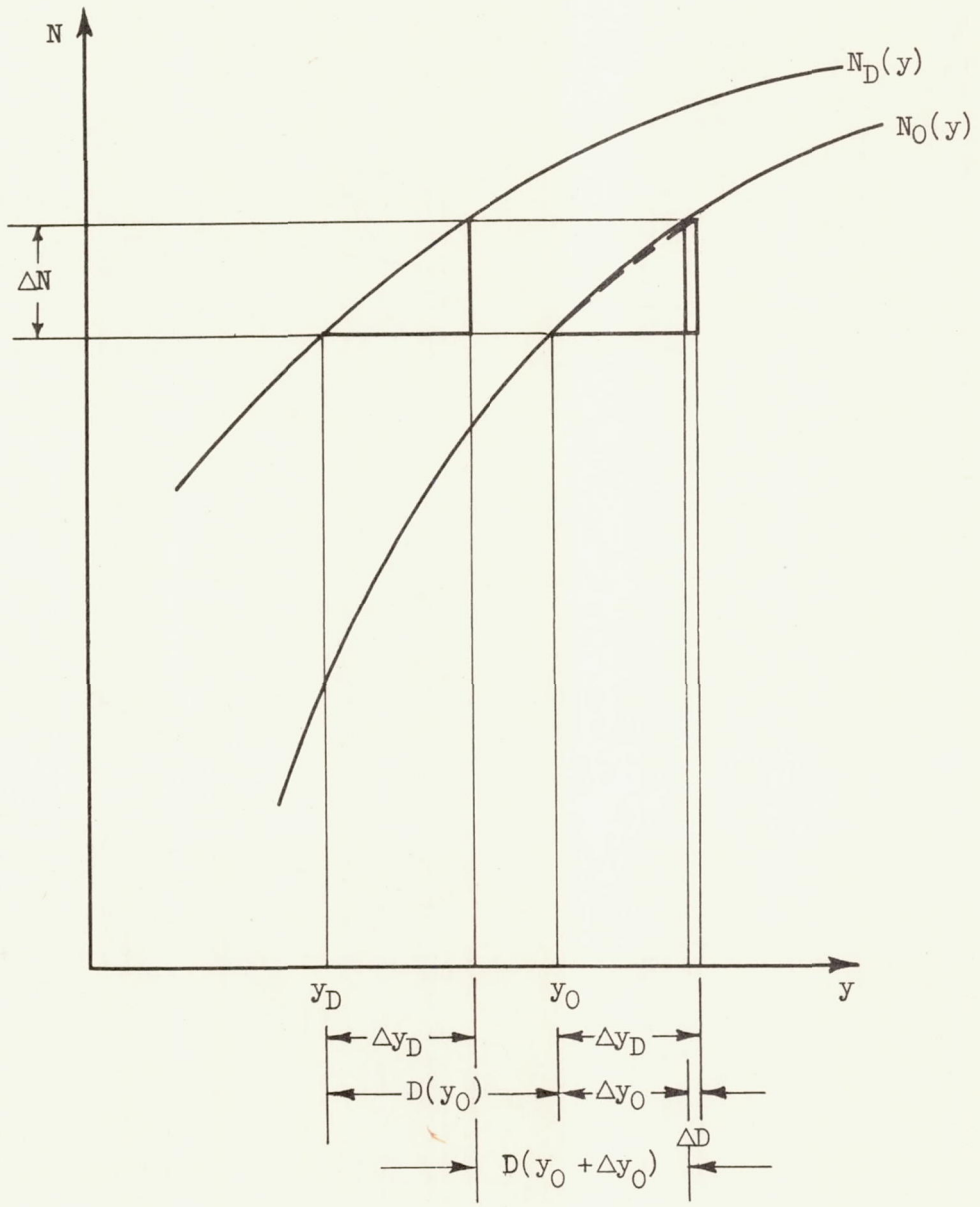
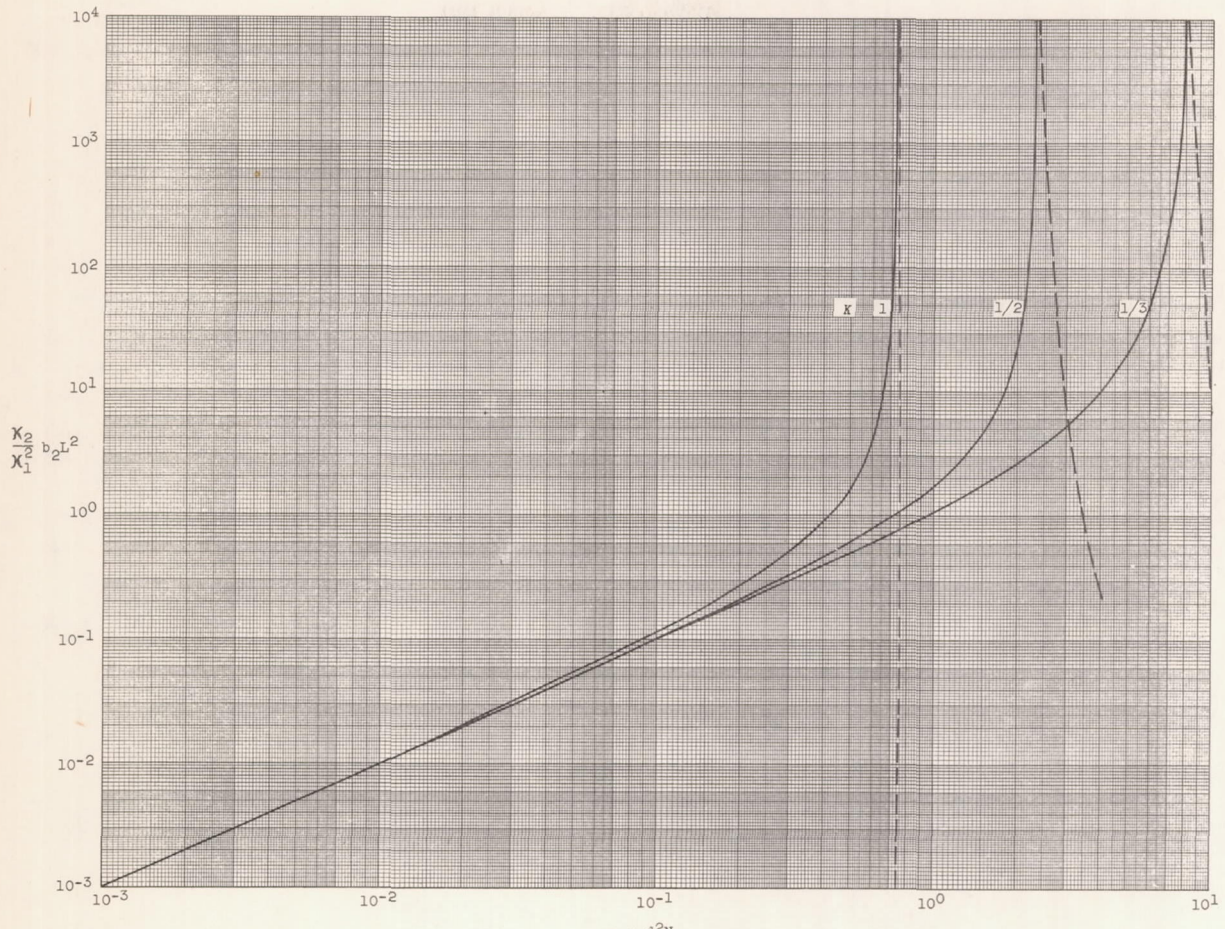
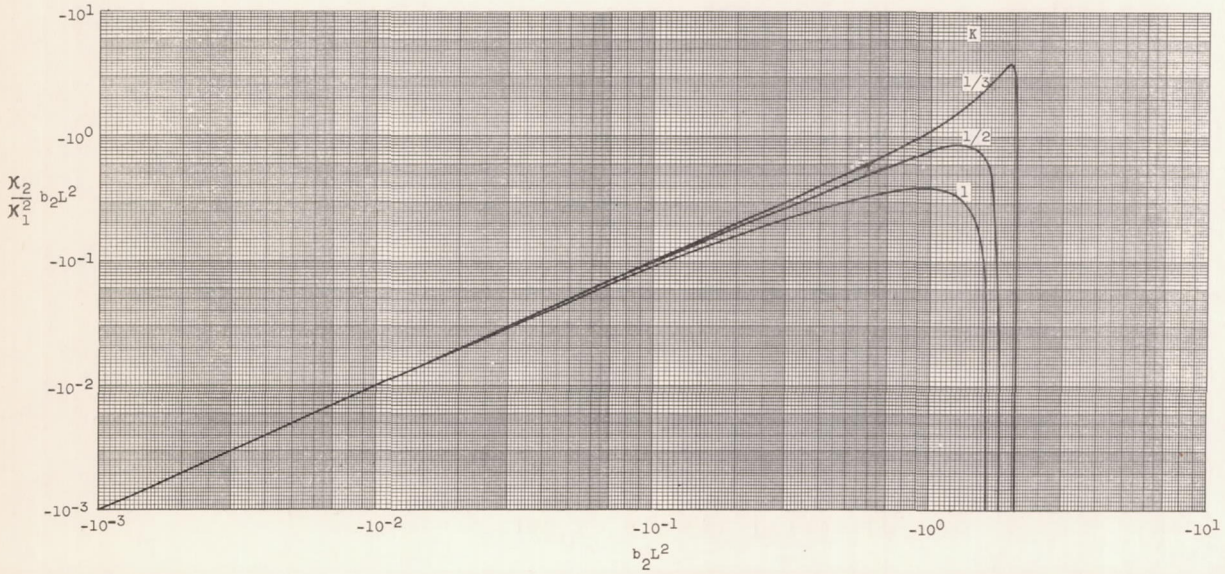


Figure 10. - Relation of observed profile $N_D(y)$ to undistorted profile $N_O(y)$.

3197



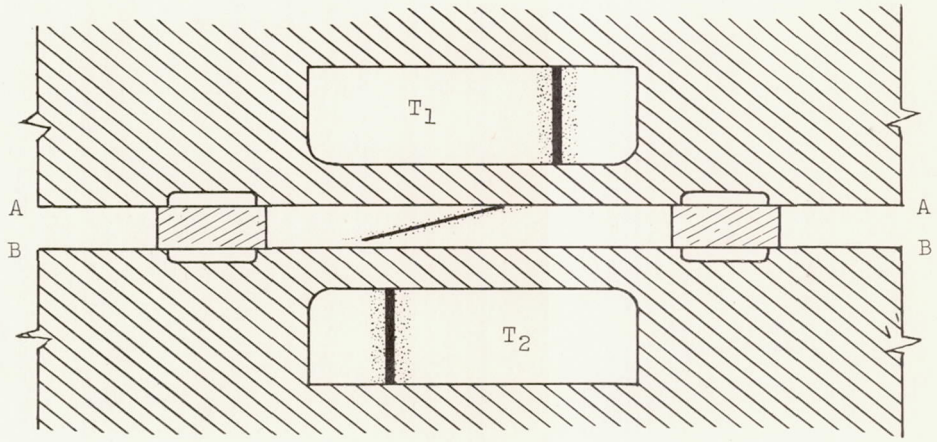
(a) $\frac{d^2N}{dy_D^2} > 0$.



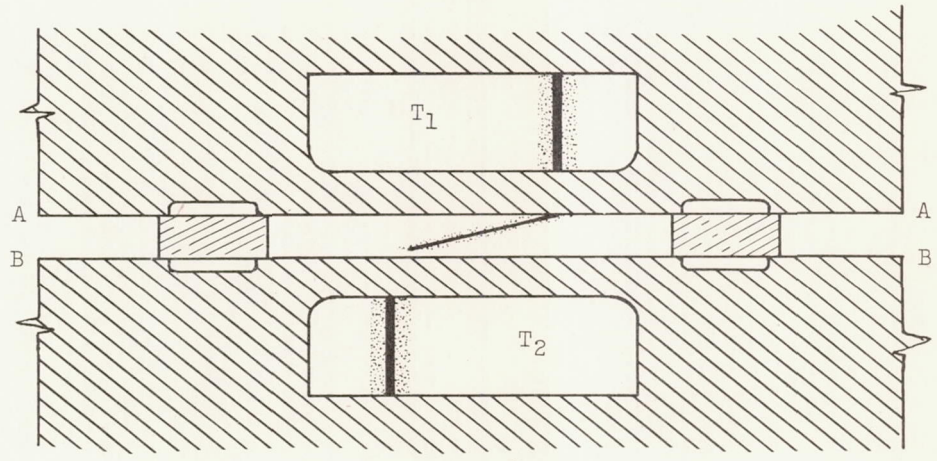
(b) $\frac{d^2N}{dy_D^2} < 0$.

Figure 11. - Graph for computing coefficient b_2.

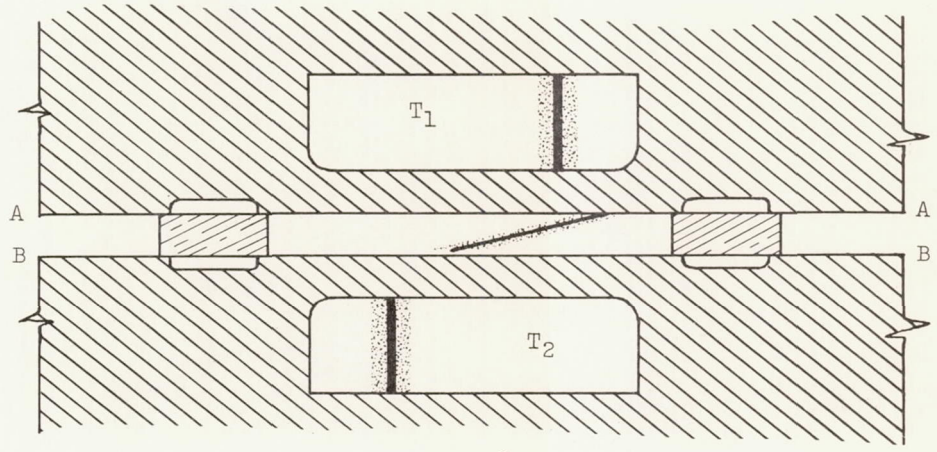
3197



(a) $K<\frac{2}{3}$.



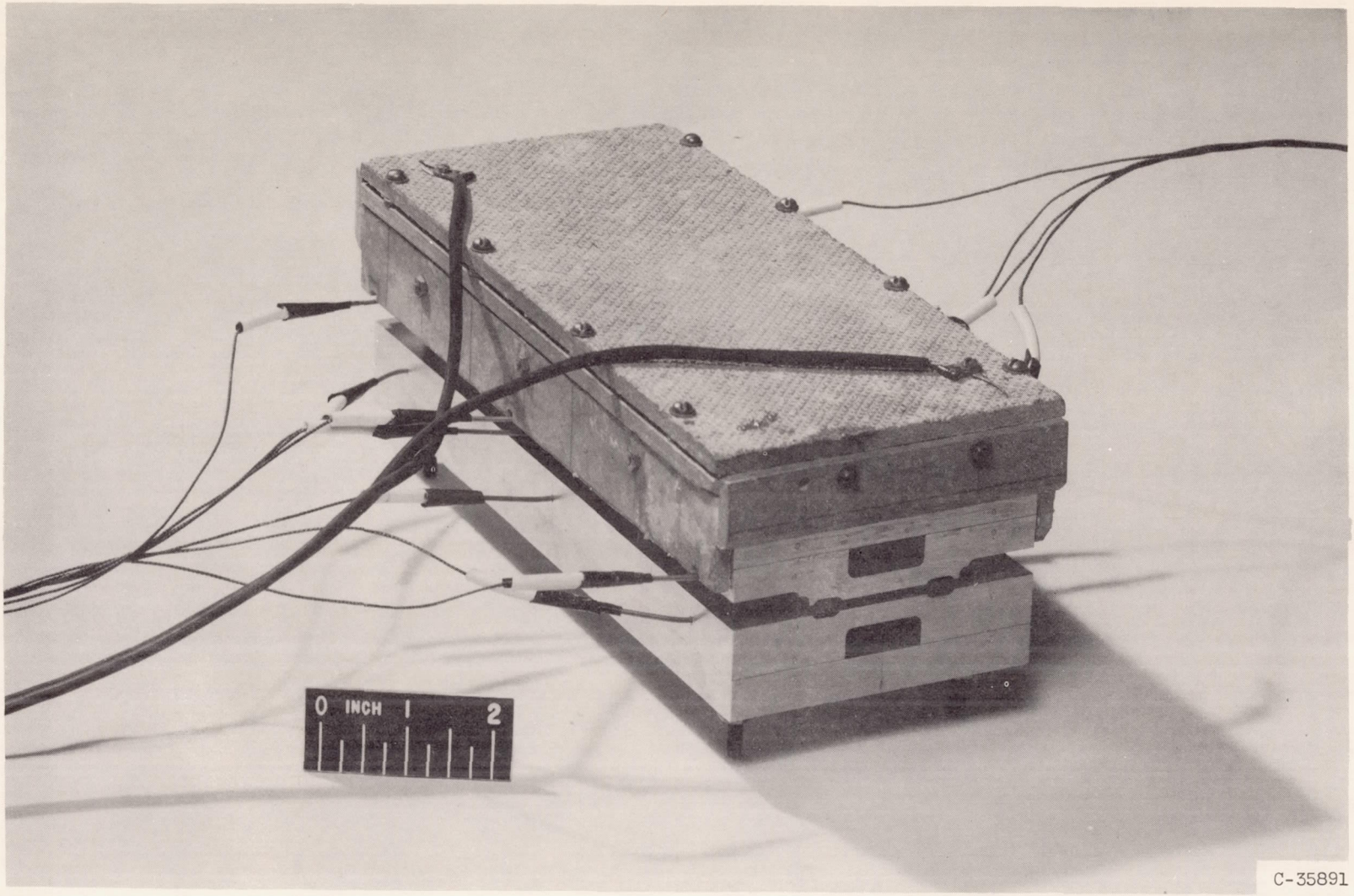
(b) $K = \frac{2}{3}$.



(c) $K>\frac{2}{3}$.

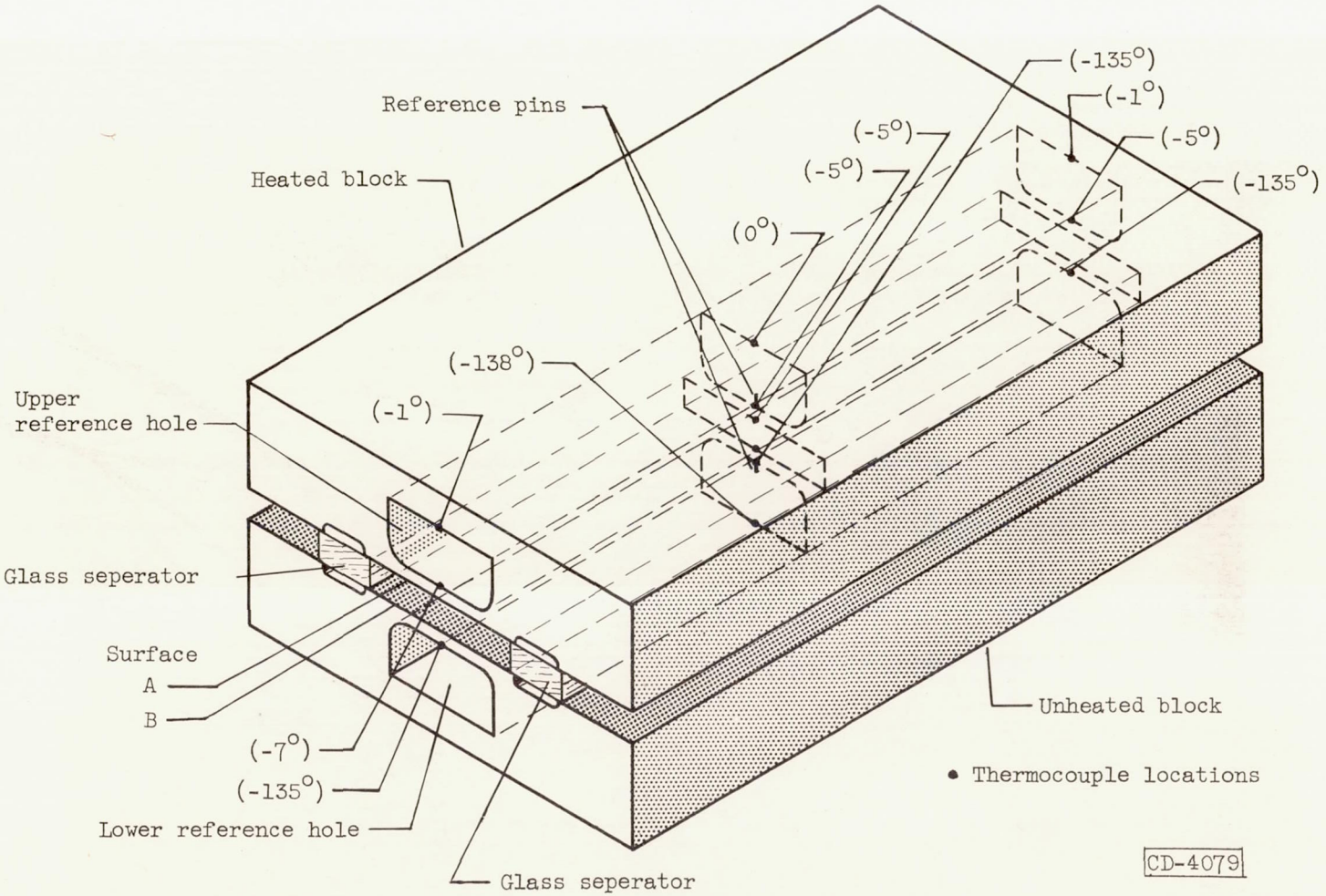
CD-4078

Figure 12. - Fringe shifts associated with various focal planes in hot-plate model.



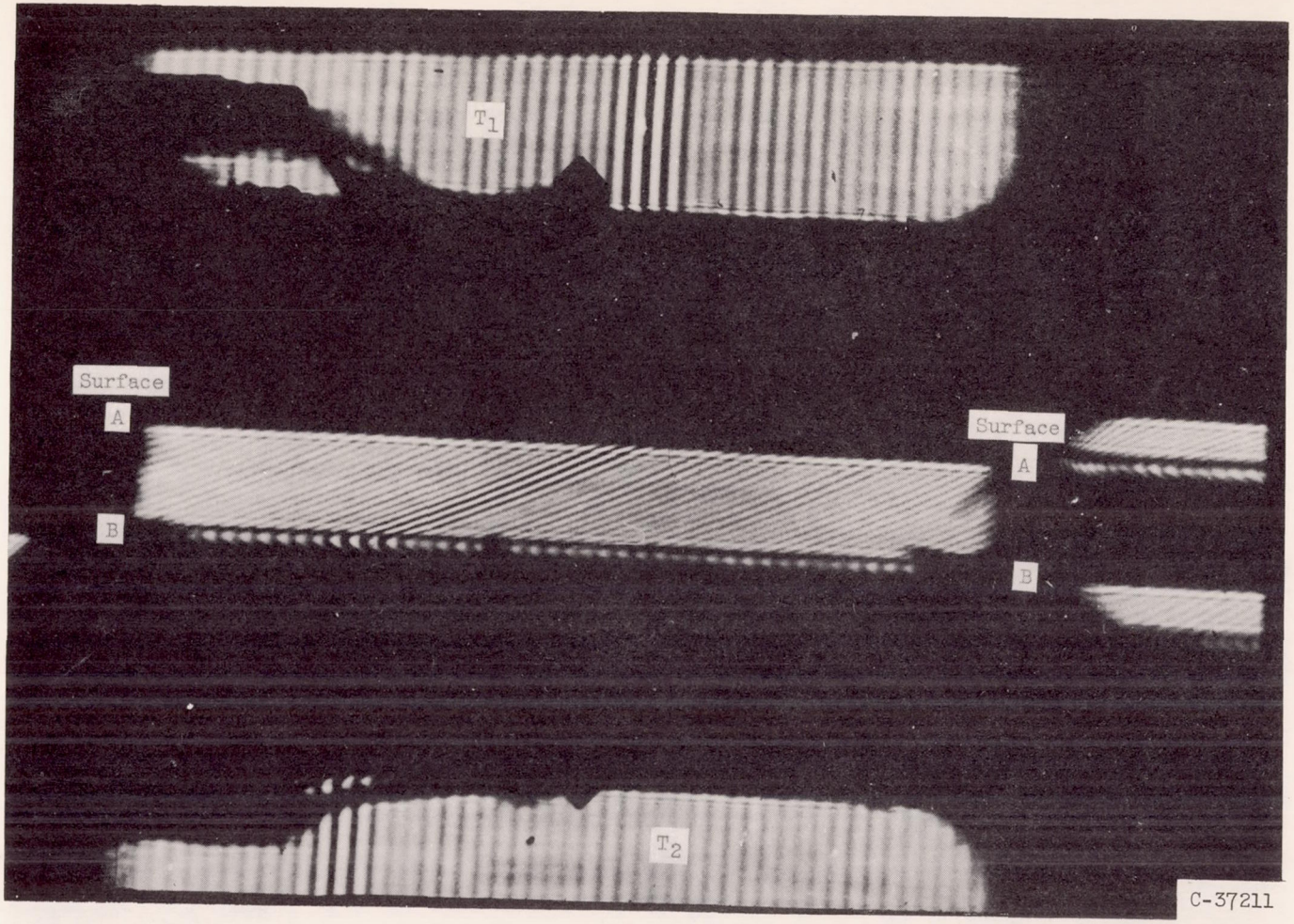
(a) Photograph.

Figure 13. - Hot-plate model.



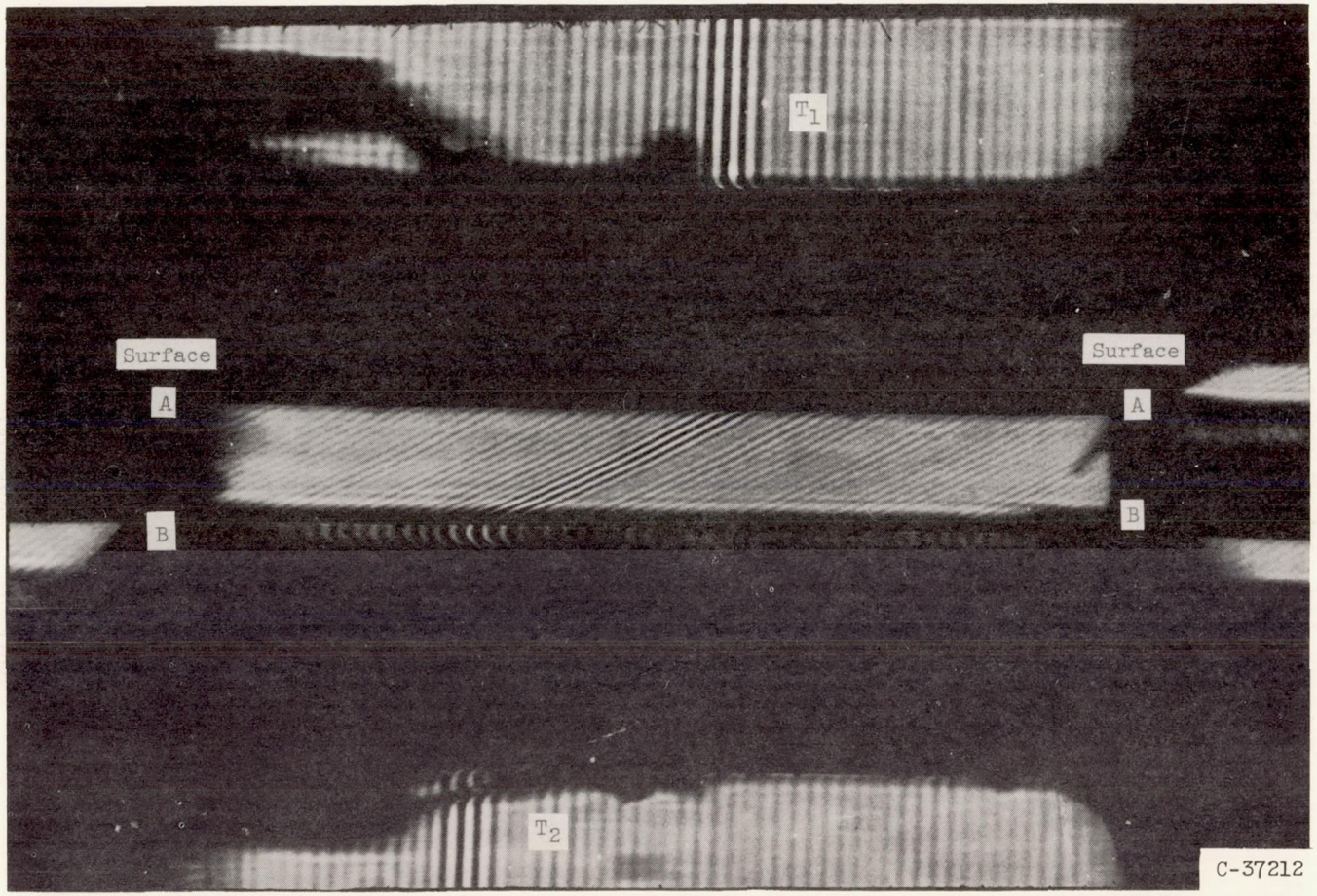
(b) Schematic diagram. (Temperature drop indicated with respect to temperature (272°F) at uppermost midspan thermocouple location.)

Figure 13. - Concluded. Hot-plate model.



(a) $K = \frac{1}{2}$.

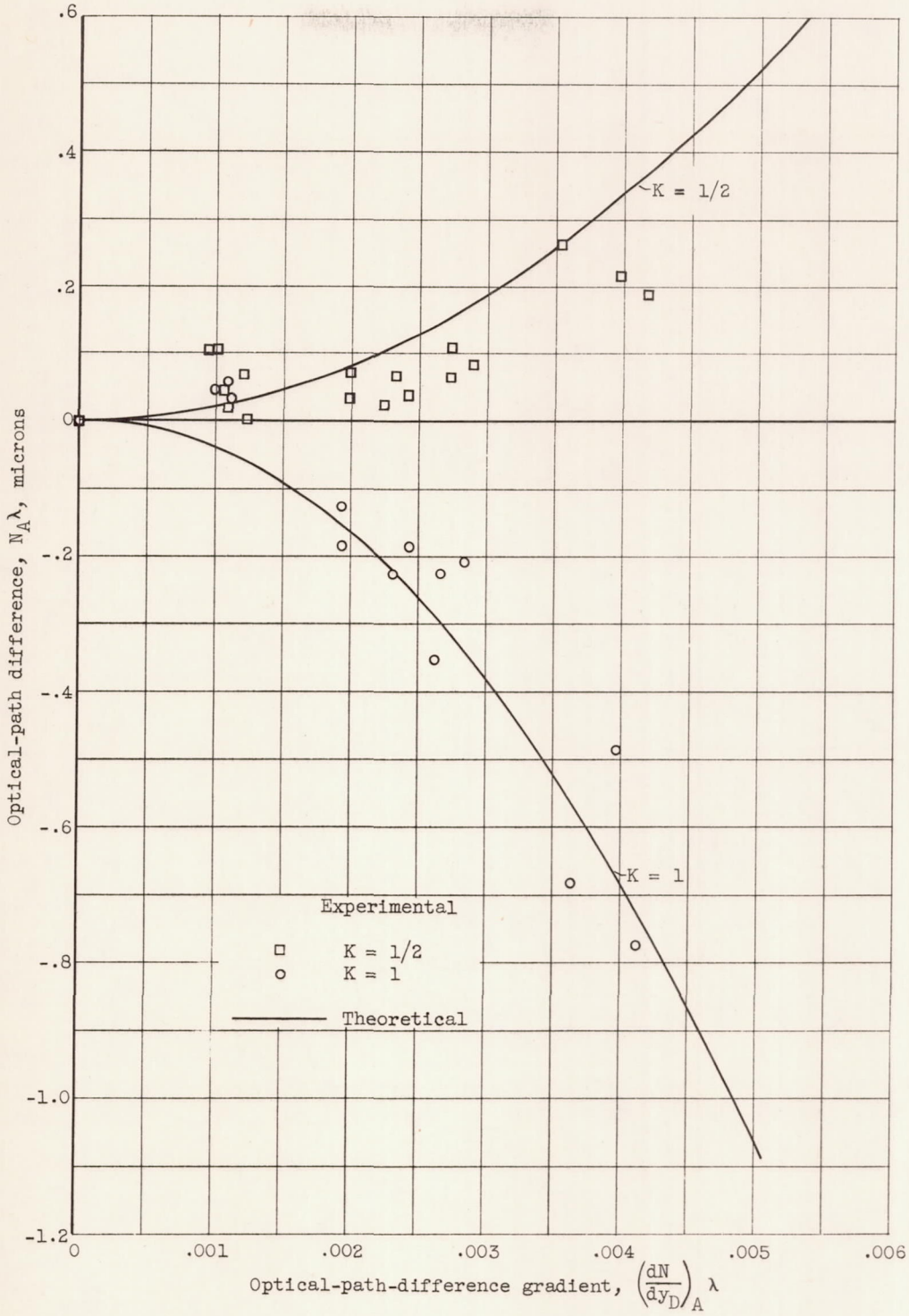
Figure 14. - Interferogram of heated model.



(b) K = 1.

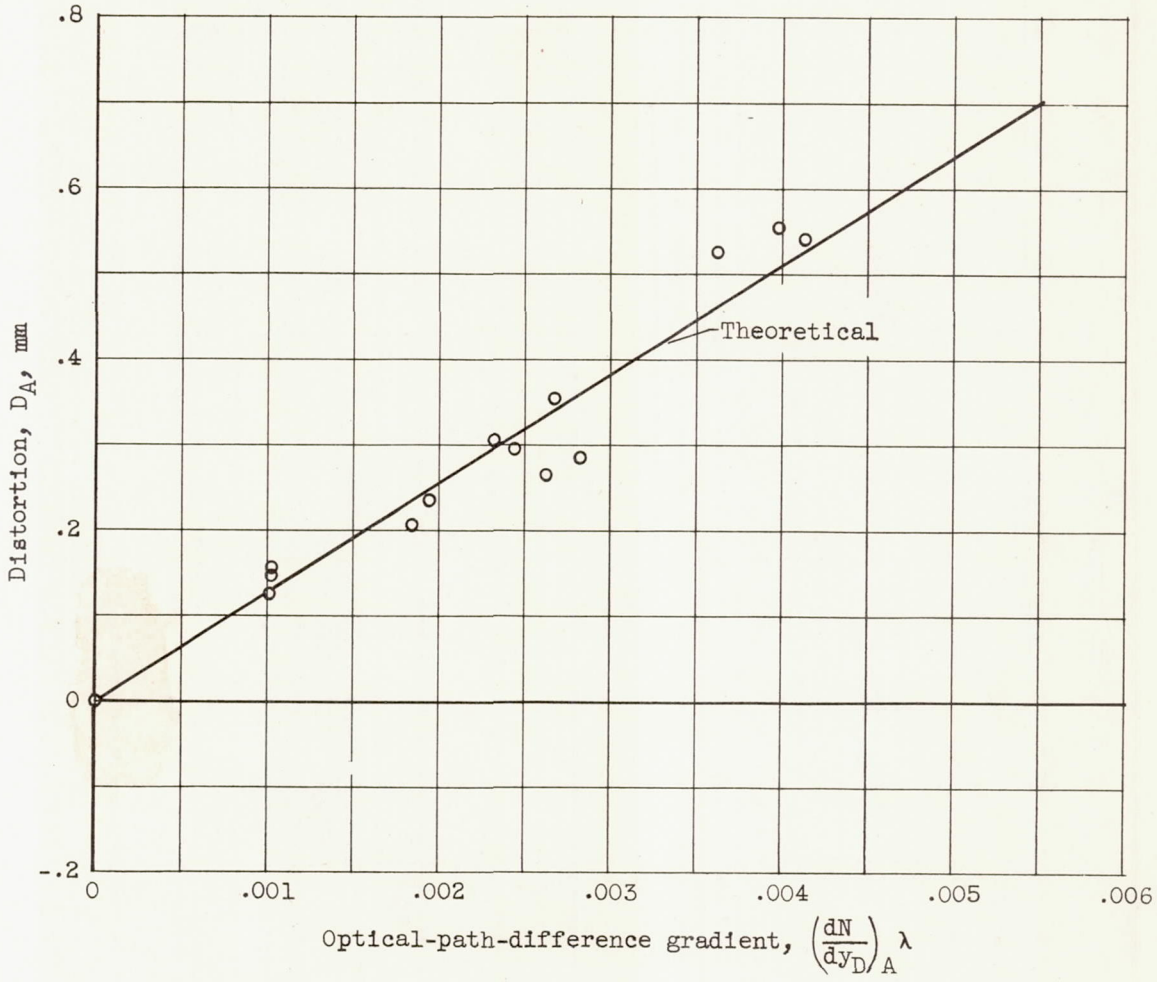
Figure 14. - Concluded. Interferogram of heated model.

3197.



(a) Optical-path differences.

Figure 15. - Verification of refraction-error formula associated with constant density gradient.



(b) Distortion; K = 1.

Figure 15. - Concluded. Verification of refraction-error formula associated with constant density gradient.

NACA-Langley - 2-25-55 - 1000